Universality classes of first-passage-time distribution in confined media

B. Meyer, C. Chevalier, R. Voituriez, and O. Bénichou
Laboratoire de Physique Théorique de la matière Condensée (UMR 7600), case courier 121, Université Paris 6, 4 place Jussieu, F-75255 Paris Cedex 05, France
(Received 10 December 2010; published 16 May 2011)

We study the first-passage time (FPT) distribution to a target site for a random walker evolving in a bounded domain. We show that in the limit of large volume of the confining domain, this distribution falls into universality classes indexed by the walk dimension d_w and the fractal dimension d_f of the medium, which have been recently identified previously [Bénichou *et al*., Nat. Chem. **2**, 472 (2010)]. We present in this paper a complete derivation of these universal distributions, discuss extensively the range of applicability of the results, and extend the method to continuous-time random walks. This analysis puts forward the importance of the geometry, and in particular the position of the starting point, in first-passage statistics. Analytical results are validated by numerical simulations, applied to various models of transport in disordered media, which illustrate the universality classes of the FPT distribution.

DOI: 10.1103/PhysRevE.83.051116 PACS number(s): 05.40.Fb, 05.40.Jc

I. INTRODUCTION

The first-passage time (FPT) of a random walker to a given target site of a domain is a quantity that is involved in the quantification of the kinetics of various processes. A striking example is given by transport limited reactions, which have been studied in various contexts [1–3]. The impact of transport on the kinetics is particularly important when a small number of reactants is involved, which is the case of many chemical reactions taking place in living cells [4–6]. Let us mention, for example, the search for their specific DNA sequences by transcription factors [7–15], which constitutes a key step in the regulation of gene expression.

In this article, we study the effect of confinement on FPT properties, keeping in mind the example of transport-limited reactions in confined media, such as reactions in cells or in subdomains of cells. More precisely, we investigate the following questions: (1) How do FPT properties depend on the volume of the confining domain? (2) How do FPT properties depend on the initial positions of the reactants? An initial answer to these questions was given in Refs. [16,17], where the mean FPT (MFPT), i.e., the first moment of the FPT probability distribution, was determined. Yet, as soon as several timescales are involved, the MFPT is not sufficient to characterize the effect of confinement on reactivity. More recently, the asymptotic form of the full distribution of the FPT has been given in Ref. [18] and discussed in the context of chemical reactivity. Here we present a complete derivation of this distribution, discuss extensively the range of applicability of the results, and extend the method to continuous-time random walks (CTRWs).

These results are applied to various models of disordered media [19,20], such as fractal networks, percolation clusters, and random-trap and and random-barrier models, and verified by numerical simulations. Such models have been frequently used to describe transport processes in real complex media, for example, in the case of exciton trapping on percolation systems [21] or in the case of anomalous motions induced by obstruction and binding in crowded environments [22–24] such as biological cells [25–29]. In particular, fractal models have regained interest in the context of the nuclear organization of DNA [30]. Indeed, recent experiments based on neutron scattering [31], rheology technics [32], and more recently the Hi-C method [33] revealed independently a fractal structure of the chromatin.

This article is organized as follows. Section II presents the derivation of the FPT probability distribution in the framework of the discrete random-walk model. Section III deals with the computation of the FPT probability distribution for the CTRW model. Section IV presents results of numerical simulations, along with discussions on the applicability of the results to the different disorder models. Finally Sec. V is dedicated to the study of the time-range validity of the theory.

II. DISCRETE-TIME RANDOM WALK

A. The model

We first introduce the model and main notations, which are chosen to be compatible with Ref. [18]. We consider a Markovian random walker evolving in a confined domain $\mathcal{D}$ of N sites. The domain $\mathcal{D}$ has a fractal structure, characterized by a fractal dimension d_f, and a characteristic length $R \propto N^{1/d_f}$; it is bounded by reflecting walls. The dynamics of the walker is characterized by the walk dimension d_w, which is defined through the scaling of the mean square displacement: $\langle \mathbf{r}^2 \rangle(t) \propto t^{2/d_w}$.

The propagator $W_{ji}(n)$, i.e., the probability that the walker, starting at $t = 0$ from site i, is at site j after n time steps, satisfies the master equation

$$W_{ji}(n) = \sum_{k=1}^{N} w_{jk}\, W_{ki}(n-1), \tag{1}$$

where w_{jk} is the transition probability from site k to site j, along with the normalization condition:

$$\sum_{j=1}^{N} W_{ji}(n) = 1, \quad \forall n. \tag{2}$$

Transition probabilities are normalized so that

$$\forall i, \ \sum_{j=1}^{N} w_{ji} = 1. \tag{3}$$

Let W_j^{stat} be the stationary probability at site j. It is assumed in the following that

(1) The stationary probability W_j^{stat} verifies

$$\forall\, j,\ W_j^{\text{stat}} \xrightarrow[N\to\infty]{} 0. \tag{4}$$

(2) The detailed balanced conditions are satisfied:

$$\forall\, i, j,\ w_{ji}\, W_i^{\text{stat}} = w_{ij}\, W_j^{\text{stat}}. \tag{5}$$

In what follows, we will make use repeatedly of the function H defined by

$$H_{ji} = \sum_{n=0}^{\infty} \left[W_{ji}(n) - W_j^{\text{stat}}\right]. \tag{6}$$

Using this definition, Eqs. (1) and (2) for W_{ji} lead to

$$\sum_{k=1}^{N} w_{jk}\, H_{ki} = H_{ji} + W_j^{\text{stat}} - \delta_{j,i} \tag{7}$$

and

$$\sum_{j=1}^{N} H_{ji} = 0. \tag{8}$$

Consequently, H can be called the pseudo-Green function of the problem [34]. It is shown in Appendix A that both the propagator of the walk and the pseudo-Green function satisfy some useful symmetry relations, under the detailed balance hypothesis (5). These relations are

$$W_{ji}(n)\, W_i^{\text{stat}} = W_{ij}(n)\, W_j^{\text{stat}} \tag{9}$$

and

$$H_{ji}\, W_i^{\text{stat}} = H_{ij}\, W_j^{\text{stat}}. \tag{10}$$

We focus on the time necessary for the walker starting from a site S to reach for the first time a given target site T. We denote by $r = |\mathbf{r}_T - \mathbf{r}_S|$ the ST distance and by P_{TS} the probability distribution of the FPT at T starting from S. Partitioning over the first step of the walk leads to the following backward equation for P_{TS} in discrete time:

$$P_{TS}(n) = \sum_{j=1}^{N} w_{jS}\, P_{Tj}(n-1). \tag{11}$$

The probability distribution P_{TS} is normalized according to

$$\sum_{n=0}^{\infty} P_{TS}(n) = 1. \tag{12}$$

We denote by $\hat{P}_{TS}$ the Laplace transform of P_{TS}, defined by

$$\hat{P}_{TS}(s) = \sum_{n=0}^{\infty} P_{TS}(n)\, \exp(-s\, n). \tag{13}$$

Expanding this expression in the neighborhood of $s = 0$ allows one to express $\hat{P}_{TS}$ in terms of the FPT moments $\langle \mathbf{T}_{TS}^k \rangle$:

$$\hat{P}_{TS}(s) = \sum_{k=0}^{\infty} \frac{(-1)^k}{k!}\, s^k \left\langle \mathbf{T}_{TS}^k \right\rangle. \tag{14}$$

Last, it will be useful to introduce the global MFPT (GMFPT) $\overline{\langle \mathbf{T} \rangle}_T$, which is defined as the average over all possible starting sites in the domain of the mean first-passage time (MFPT) $\langle \mathbf{T}_{TS} \rangle$:

$$\overline{\langle \mathbf{T} \rangle}_T = \sum_{j=1}^{N} W_j^{\text{stat}}\, \langle \mathbf{T}_{Tj} \rangle. \tag{15}$$

B. Moments of the first-passage time (FPT)

1. Exact recurrence relation

It can be shown (see Ref. [18] and Appendix B) that by Laplace transforming Eq. (11) the following hierarchy of equations for the FPT moments can be obtained:

$$-\sum_{j=1}^{N} w_{jS}\left(\left\langle \mathbf{T}_{Tj}^n \right\rangle - \left\langle \mathbf{T}_{TS}^n \right\rangle\right) = \sum_{k=1}^{n} \binom{n}{k} (-1)^{k+1} \left\langle \mathbf{T}_{TS}^{n-k} \right\rangle. \tag{16}$$

An explicit solution of this hierarchy of equations is derived in Appendix B (see also Ref. [18]) and reads

$$\left\langle \mathbf{T}_{TS}^n \right\rangle = \frac{1}{W_T^{\text{stat}}} \sum_{j=1}^{N} \sum_{k=1}^{n} \binom{n}{k} (-1)^{k+1} + \left[(H_{TT} - H_{TS}) W_j^{\text{stat}} (H_{jS} - H_{jT}) W_T^{\text{stat}}\right] \left\langle \mathbf{T}_{Tj}^{n-k} \right\rangle. \tag{17}$$

Note that Eq. (17) with $n = 0$ allows one to recover the equation for the mean FPT [17]:

$$\langle \mathbf{T}_{TS} \rangle = \frac{1}{W_T^{\text{stat}}}\, (H_{TT} - H_{TS}). \tag{18}$$

Inserting this expression into the definition of the GMFPT (15) and using the symmetry relation (9) yields [35]

$$\overline{\langle \mathbf{T} \rangle}_T = \frac{H_{TT}}{W_T^{\text{stat}}}, \tag{19}$$

which will be used later.

2. Asymptotic expression for large N

Hitherto results are exact. We now restrict our attention to the large-volume limit $N \to \infty$, or equivalently $R \gg r$. This approximation, which is convenient for the calculation of the entire first-passage probability distribution, deserves an important remark about its validity: In practice, the results reveal a very good agreement with numerical simulations even for small network sizes (sometimes $N < 100$; see Fig. 7 for a striking example). We recall that we focus on the physically reasonable case where the stationary probability tends toward zero in this large-volume limit [Eq. (4)]. In that case, as we will see later in this section, the moments satisfy

$$\frac{\left\langle \mathbf{T}_{TS}^{k-1} \right\rangle}{\left\langle \mathbf{T}_{TS}^{k} \right\rangle} \xrightarrow[N\to\infty]{} 0. \tag{20}$$

In the large-volume limit, the recurrence relation (17) thus simplifies to

$$\left\langle \mathbf{T}_{TS}^n \right\rangle \sim \frac{n}{W_T^{\text{stat}}} \sum_{j=1}^{N} \left[(H_{TT} - H_{TS}) W_j^{\text{stat}} + (H_{jS} - H_{jT}) W_T^{\text{stat}}\right] \left\langle \mathbf{T}_{Tj}^{n-1} \right\rangle, \tag{21}$$

where $\sim$ denotes equivalence for large N. Using this recurrence equation, we now determine the explicit expression for the kth FPT moment. To do so, we distinguish between two types of exploration of the confining domain by the walker.

Noncompact exploration ($d_w < d_f$). In the case of noncompact exploration [36], where the mean number of distinct sites visited by the walker in the absence of confinement increases linearly with the time, it can be shown that the mean number of visits of site j by the walker starting from site i is finite [37]. In other words, the large-volume limit of the pseudo-Green function H, i.e., the Green function G, given by

$$G_{ji} = \sum_{n=0}^{\infty} W_{ji}^{\infty}(n), \tag{22}$$

where W_{ji}^{∞} stands for the propagator of the walk in unbounded space, is finite. Hence, one can approximate, in the large-volume limit, the pseudo-Green function H by the Green function G. By using a recurrence reasoning based on relation (21) and making the assumption that

$$\sum_{k=1}^{N} H_{Tk}\,(H_{kT} - H_{kS}) = \mathcal{O}\Big[\big(W_T^{\rm stat}\big)^{-1-\frac{2}{d_f}(d_w-d_f)}\Big], \tag{23}$$

we demonstrate in Appendix E that the FPT moments read, in the large-volume limit:

$$\big\langle \mathbf{T}_{TS}^n \big\rangle = n!\,\overline{\langle \mathbf{T}\rangle}_T^{\,n}\,\frac{H_{TT}-H_{TS}}{H_{TT}} + \mathcal{O}\Big[\big(W_T^{\rm stat}\big)^{-n-\frac{2}{d_f}(d_w-d_f)}\Big]. \tag{24}$$

Let us put forward that assumption (23) is valid in a large range of situations. For instance, we show in Appendix E that it is verified for the general example of a scale-invariant problem, in which the unbounded propagator satisfies the standard scaling [19]:

$$W_{ji}(n) \sim n^{-d_f/d_w}\, f\left(\frac{|\mathbf{r}_j - \mathbf{r}_i|}{n^{1/d_w}}\right), \tag{25}$$

and in which the stationary probability is uniform:

$$W_j^{\rm stat} = \frac{1}{N},\ \forall j. \tag{26}$$

Compact exploration ($d_w > d_f$). In the case of compact exploration [36], the mean number of visits of site j by the walker starting from site i is infinite in absence of confinement, i.e., the sum $\sum_{n=0}^{\infty} W_{ji}^{\infty}(n)$ now diverges, and the Green function G_{ji}, which constitutes the leading-order term of the pseudo-Green function in the large-volume limit, is therefore not defined. Note, however, that differences of pseudo-Green functions have a well-defined large-volume limit, which proves to be useful in calculating the first moment of the FPT [17]. In the study of higher moments, pseudo-Green functions themselves, and not only differences, are involved. It is therefore necessary to go further than the leading-order term.

To do so, we focus on the large-volume limit and make use of a continuous-time formalism. This can be justified by the fact that all timescales involved in the problem (such as $\overline{\langle \mathbf{T}\rangle}_T$ or $\langle \mathbf{T}_{TS}\rangle$) diverge with the system size N, so that the elementary time step is much smaller than all timescales of the problem. Note that in continuous time the FPT distribution is a density and therefore has units of inverse time, while in a discrete setting it is dimensionless. In the remainder of the article, both formalisms will therefore be used indiscriminately.

In order to determine the dependence of the pseudo-Green function with the volume of the confining domain, we use the O'Shaughnessy-Procaccia transport equation [38,39], which describes the evolution of the probability density $W(r,t|0)$ of a random walker evolving in a fractal domain. It is shown in detail in Appendix D that we get, from this equation, the following expression for the pseudo-Green function H in the large-volume limit:

$$H_{TT} \sim \frac{2d_f R^{d_w-d_f}}{K\Omega d_w\big(d_w^2-d_f^2\big)}, \tag{27a}$$

$$H_{TT} - H_{TS} \sim \frac{r^{d_w-d_f}}{K\,\Omega\,d_f\,(d_w-d_f)}, \tag{27b}$$

$$\overline{\langle \mathbf{T}\rangle}_T \sim \frac{2\,d_f\,R^{d_w}}{K\,d_w\,\big(d_w^2-d_f^2\big)}, \tag{27c}$$

where K is the generalized diffusion coefficient and Ω is defined by $N = \Omega\,R^{d_f}$. Using the recurrence relation (17) and evaluating the orders of magnitude of the various terms involved in each iteration step with the help of the above expressions (see Appendix E for detailed calculations), we finally get, for the five first FPT moments in the large-volume limit:

$$\big\langle \mathbf{T}_{TS}^n \big\rangle \sim n!\,c_n\,\overline{\langle \mathbf{T}\rangle}_T^{\,n}\,\frac{H_{TT}-H_{TS}}{H_{TT}}, \tag{28}$$

with

$$c_1 = 1,\quad c_2 = 1,\quad c_3 = \frac{(5d_w-2d_f)(d_f+d_w)^2}{4d_f\big(4d_w^2-d_f^2\big)}. \tag{29}$$

The expressions of c_4 and c_5 are given in Appendix C.

C. FPT probability distribution.

Using the above determination of the FPT moments, we now derive the asymptotic expressions of the FPT distribution in both noncompact and compact cases, which were first given in Ref. [18].

Noncompact exploration We deduce directly from expression (24) of the FPT moments the expression of the FPT probability distribution in the large-volume limit:

$$P_{TS}(t) = \left(1 - \frac{\langle \mathbf{T}_{TS}\rangle}{\overline{\langle \mathbf{T}\rangle}_T}\right)\delta(t) + \frac{\langle \mathbf{T}_{TS}\rangle}{\overline{\langle \mathbf{T}\rangle}_T}\,\phi(t), \tag{30}$$

where

$$\phi(t) = \frac{1}{\overline{\langle \mathbf{T}\rangle}_T}\,\exp\left(-\frac{t}{\overline{\langle \mathbf{T}\rangle}_T}\right). \tag{31}$$

Compact exploration. Let us consider the following function $M_{TS}(s)$ for $s > 0$:

$$M_{TS}(s) = 1 - \frac{2d_f^2}{d_w(d_w+d_f)}\,\frac{\langle \mathbf{T}_{TS}\rangle}{\overline{\langle \mathbf{T}\rangle}_T}\,\tilde{\chi}(s), \tag{32}$$

where

$$\tilde{\chi}(s) = \frac{2^{\nu-1}\, d_f^{\nu-1}\, d_w^{\nu-1}}{\left(d_w^2 - d_f^2\right)^{\nu-1}} \frac{\Gamma(\nu)}{\Gamma(2-\nu)} \left(s\, \overline{\langle \mathbf{T} \rangle}_T\right)^{1-\nu} \times \frac{I_\nu\left[\sqrt{\frac{2\left(d_w^2 - d_f^2\right)}{d_w\, d_f}} \sqrt{s\, \overline{\langle \mathbf{T} \rangle}_T}\right]}{I_{-\nu}\left[\sqrt{\frac{2\left(d_w^2 - d_f^2\right)}{d_w\, d_f}} \sqrt{s\, \overline{\langle \mathbf{T} \rangle}_T}\right]}, \tag{33}$$

with $\nu = d_f/d_w$. This function is the large-volume limit of the Laplace transform $\hat{P}_{TS}(s)$ of the first-passage probability distribution, as we discuss below and in Appendix D.

Function (32) is introduced because its first five moments are exactly given by (28) along with (29), as can be checked explictly. We assume that this agreement remains true for any arbitrary (finite) order of the expansion.

Note that the large-volume approximation (32) is obtained by taking the limit $(\frac{r}{R})^{d_w} \overline{\langle \mathbf{T} \rangle}_T s \ll 1$. Hence it holds only when the Laplace parameter s is small enough, which corresponds to the large time limit. We defer to Sec. V the quantitative determination of the time-range validity of our results, as well as the instructive example of the unidimensional problem.

The large-volume limit implies here that the function (32) is not a Laplace transform of a regular function, because for $\nu < 1$ (compact exploration) one has $\tilde{\chi}(s) \xrightarrow[s\to\infty]{} \infty$. This difficulty can be circumvented by introducing the auxiliary function:

$$M_{TS}^{\sigma}(s) = 1 - \frac{2d_f^2}{d_w(d_w + d_f)} \frac{\langle \mathbf{T}_{TS} \rangle}{\overline{\langle \mathbf{T} \rangle}_T} \tilde{\chi}^{\sigma}(s), \tag{34}$$

$$\text{with} \quad \hat{\chi}^{\sigma}(s) = e^{-s/\sigma} \tilde{\chi}(s), \quad \sigma > 0, \tag{35}$$

which is a well-defined Laplace transform satisfying

$$M_{TS}^{\sigma}(s) \xrightarrow[\sigma\to\infty]{} M_{TS}(s). \tag{36}$$

The inverse Laplace transform of $\hat{\chi}^{\sigma}(s)$ and therefore $M_{TS}^{\sigma}(s)$ is given in detail in Appendix F. Finally one obtains

$$P_{TS}(t) = \left[1 - \frac{2d_f^2}{d_w(d_f + d_w)} \frac{\langle \mathbf{T}_{TS} \rangle}{\overline{\langle \mathbf{T} \rangle}_T}\right] \delta(t) + \frac{2d_f^2}{d_w(d_f + d_w)} \frac{\langle \mathbf{T}_{TS} \rangle}{\overline{\langle \mathbf{T} \rangle}_T} \phi(t) \tag{37a}$$

$$\text{with} \quad \phi(t) \sim \chi(t) \quad \text{for} \quad t \gg t_c, \tag{37b}$$

where

$$\chi(t) = \frac{1}{\overline{\langle \mathbf{T} \rangle}_T} \frac{d_f d_w}{\left(d_w^2 - d_f^2\right) 2^{2-2\nu}} \frac{\Gamma(\nu)}{\Gamma(2-\nu)} \times \sum_{k=0}^{\infty} \alpha_k^{3-2\nu} \frac{J_\nu(\alpha_k)}{J_{-\nu+1}(\alpha_k)} \exp\left[-\frac{\alpha_k^2 d_w d_f}{2\left(d_w^2 - d_f^2\right)} \frac{t}{\overline{\langle \mathbf{T} \rangle}_T}\right], \tag{38a}$$

$$t_c = \frac{2\left(d_w^2 - d_f^2\right)}{d_w d_f} \left(\frac{r}{R}\right)^{d_w} \overline{\langle \mathbf{T} \rangle}_T. \tag{38b}$$

In the relations above, $\alpha_0 < \alpha_1 < \cdots$ are the real zeros of $J_{-\nu}$; t_c is calculated in Sec. V; and ϕ is a normalized function (whereas χ is not).

Universality classes of FPT distributions Let us focus on the expressions (30) and (37). One can immediately see that both formulas can be gathered into a single common expression. In particular, for the sake of notation simplicity, $\phi(t)$, $\hat{\phi}(s)$, and the other quantities that are denoted by the same symbol for both exploration types will be referred to indiscriminately. Henceforth, one needs only to be cautious that in the case of compact exploration, the time (or Laplace parameter) range is restricted, following Eq. (101).

These expressions make it clear that the natural time variable to use is the rescaled variable θ defined by

$$\theta = \frac{t}{\overline{\langle \mathbf{T} \rangle}_T}. \tag{39}$$

Let Q_{TS} be the FPT probability distribution for θ. We have, for the two types of exploration, in the large-volume limit:

$$Q_{TS}(\theta) = (1 - \Pi_{TS})\, \delta(\theta) + \Pi_{TS}\, \psi(\theta), \tag{40}$$

which characterizes universality classes of FPT distributions in confined media.

The dependence on the reduced time θ is fully contained in the functions δ and ψ, while the spatial dependence on r lies entirely in the function Π_{TS}, which we consequently call the geometric factor. Last, the dependence on N enters both the reduced time θ and the geometric factor Π_{TS}. The specific shape of the function ψ and that of the geometric factor Π_{TS} characterize the type of exploration (noncompact or compact).

For the noncompact exploration, which qualitatively corresponds to trajectories leaving many sites unvisited, one has

$$\psi(\theta) = \exp(-\theta), \tag{41a}$$

$$\overline{\langle \mathbf{T} \rangle}_T = \frac{H_{TT}}{W_T^{\text{stat}}} \propto N, \tag{41b}$$

$$\Pi_{TS} = \frac{\langle \mathbf{T}_{TS} \rangle}{\overline{\langle \mathbf{T} \rangle}_T} \propto 1 - \left(\frac{a}{r}\right)^{d_f - d_w}, \tag{41c}$$

where a is a typical length of the order of one step size. We have used that H_{TT} remains finite in the large-volume limit [see comment before Eq. (22)] and the scaling form of the first moment of the FPT [17,35].

In the case of compact exploration, using the scaling forms given by Eq. (27), we get

$$\psi(\theta) \sim \zeta(\theta) \quad \text{for} \quad \theta \gg \theta_c, \tag{42a}$$

$$\text{with} \quad \zeta(\theta) = \frac{2\, d_f\, d_w}{d_w^2 - d_f^2} \frac{\Gamma(\nu)}{\Gamma(2-\nu)} \sum_{k=0}^{\infty} \left(\frac{\alpha_k}{2}\right)^{3-2\nu} \times \frac{J_\nu(\alpha_k)}{J_{1-\nu}(\alpha_k)} \exp\left[-\frac{\alpha_k^2\, d_w\, d_f}{2\left(d_w^2 - d_f^2\right)} \theta\right], \tag{42b}$$

$$\overline{\langle \mathbf{T} \rangle}_T = \frac{H_{TT}}{W_T^{\text{stat}}} \propto N^{d_w/d_f}, \tag{42c}$$

$$\Pi_{TS} = \frac{2d_f^2}{d_w(d_f + d_w)} \frac{\langle \mathbf{T}_{TS} \rangle}{\overline{\langle \mathbf{T} \rangle}_T} \propto \left(\frac{r}{R}\right)^{d_w - d_f}, \tag{42d}$$

and [after Eq. (101)]:

$$\theta_c = \frac{2\left(d_w^2 - d_f^2\right)}{d_w d_f}\left(\frac{r}{R}\right)^{d_w}. \tag{43}$$

Finally, in the marginal case, i.e., when $d_f = d_w$, we obtain using the same method (details are not given here for the sake of readability) an exponential scaling function ψ as for the noncompact case, with logarithmic corrections in the volume dependence of $\overline{\langle \mathbf{T} \rangle}_T$ as well as in the volume and source-target dependencies of Π_{TS}. More explicitly one gets

$$\psi(\theta) = e^{-\theta}, \tag{44a}$$

$$\overline{\langle \mathbf{T} \rangle}_T = \frac{H_{TT}}{W_T^{\text{stat}}} \propto N \ln N, \tag{44b}$$

$$\Pi_{TS} = \frac{\langle \mathbf{T}_{TS} \rangle}{\overline{\langle \mathbf{T} \rangle}_T} \propto \frac{\beta - \ln(r)}{\beta - \ln(R)}, \tag{44c}$$

where β is a lattice-dependent constant.

Discussion. First, a few comments about expression (40). (1) Strikingly, the FPT distribution is entirely determined as soon as the first-moment $\langle \mathbf{T}_{TS} \rangle$ and averaged first-moment $\overline{\langle \mathbf{T} \rangle}_T$ of the FP distribution are known. (2) The first term (Dirac δ function) in the right-hand side takes into account trajectories reaching the target site within a time $t \ll \overline{\langle \mathbf{T} \rangle}_T$ (corresponding to $\theta \ll 1$), which more precisely scales as $t \propto \mathcal{O}(r^{d_w})$. Such trajectories can be interpreted as trajectories reaching the target site before touching the boundaries, and the factor $1 - \Pi_{TS}$ can be seen as the weight of these trajectories. On the other hand, the second term describes trajectories reaching the boundaries before the target, with weight Π_{TS}.

Let us now discuss the differences between the two types of exploration, starting with their temporal dependance held by $\psi(\theta)$. In the noncompact case, one can see that, for $t > 0$, when the source-target distance r is much larger than the step size a, the FPT distribution reduces to a simple time-decreasing exponential with weight unity. Remarkably, the exponential form for the function ψ holds universally for any values of the dimensions d_f and d_w satisfying $d_w < d_f$. As will be shown in Sec. IV, transport processes as varied as regular diffusion in three dimensions (for which $d_w = 2$ and $d_f = 3$), anomalous diffusion on supercritical percolation cluster, as well as transport in some quenched disordered media, fall into that universality class. The single-exponential scaling of ψ with time could be expected since both $\overline{\langle \mathbf{T} \rangle}_T$ and $\langle \mathbf{T}_{TS} \rangle$ [17] scale linearly with N. In the compact case, on the other hand, the function ψ is not given by a single exponential, as for the noncompact case, but rather exhibits a countable infinity of timescales, which range between r^{d_w} and R^{d_w}. This complex behavior, parametrized by d_w and d_f, is induced by the interplay between the characteristic times $\overline{\langle \mathbf{T} \rangle}_T$ and $\langle \mathbf{T}_{TS} \rangle$, which do not share the same dependence on N. Note that most fractal sets (even if embedded in 3D space, like the critical percolation cluster) lead to compact exploration.

Let us now focus on the r dependence of Π_{TS}. As expected one finds that Π_{TS} increases with r in both cases; i.e., the further the source from the target, the higher the probability to reach the boundaries before the target site. In the noncompact case, that dependence of Π_{TS} on r is significant only for r of the order of the step size a and is lost for $r \gg a$. In the compact case, on the other hand, Π_{TS} increases with r and quite remarkably tends to 0 for r small. Overall the dependence on r of the geometric weight is important for all values of r, in contrast with the noncompact case. This suggests that in the case of compact exploration, the initial distance between the reactants plays a crucial role in the kinetics of transport-limited reactions. The latter comment is reflected by the scaling of the reduced variance $(\langle \mathbf{T}_{TS}^2 \rangle - \langle \mathbf{T}_{TS} \rangle^2)/\langle \mathbf{T}_{TS} \rangle^2$: In the case of noncompact exploration that quantity is of order 1 at any distance, whereas in the compact case it scales like $(R/r)^{d_w - d_f}$, so that very large fluctuations occur when $r \ll R$.

III. CONTINUOUS-TIME RANDOM WALK

A. The model

So far, we considered a discrete-time random walker evolving on a fractal lattice. A very useful extension of this model consists in assuming that there exists a finite, random-time interval between two consecutive jumps of the walker. This model is usually referred to as the continuous-time random-walk (CTRW) model [20]. We first recall the simple connection between CTRWs and discrete time random walks studied above for first-pasxsage properties [37,40].

The waiting time between two jumps is described as a continuous random variable, whose probability distribution is denoted by $F(t)$. Let us denote by $F_j(t)$ the probability distribution that the jth step is realized at time t knowing that the walker performed the first step at time $t = 0$. We have [37]

$$F_j(t) = \int_0^t F(t - t')\, F_{j-1}(t')\, dt', \tag{45}$$

which yields, in Laplace space,

$$\hat{F}_j(s) = \hat{F}(s)\, \hat{F}_{j-1}(s), \tag{46}$$

with $\hat{F}_1(s) = \hat{F}(s)$. We thus get, iteratively,

$$\hat{F}_j(s) = \hat{F}^j(s). \tag{47}$$

Let $\mathcal{P}_{TS}$ be the first-passage time probability distribution of the CTRW and $\hat{\mathcal{P}}_{TS}$ its Laplace transform. To determine $\hat{\mathcal{P}}_{TS}$, we shall link it to the already known FPT probability distribution P_{TS} of the discrete-time random-walk model. Indeed, the distribution $\mathcal{P}_{TS}$ satisfies [37]

$$\mathcal{P}_{TS}(t) = \sum_{n=1}^{\infty} P_{TS}(n)\, F_n(t). \tag{48}$$

Laplace transforming this equation gives

$$\hat{\mathcal{P}}_{TS}(s) = \sum_{n=1}^{\infty} P_{TS}(n) \hat{F}^n(s). \tag{49}$$

Equivalently, one has

$$\hat{\mathcal{P}}_{TS}(s) = G_{TS}[\hat{F}(s)], \tag{50}$$

where G_{TS} is the generating function of P_{TS}. In terms of the discrete Laplace transform defined in (13) it reads

$$\begin{aligned} \hat{\mathcal{P}}_{TS}(s) &= \hat{P}_{TS}[-\ln(\hat{F}(s))] \\ &= (1 - \Pi_{TS}) + \Pi_{TS}\, \hat{\phi}\{-\ln[\hat{F}(s)]\}, \end{aligned} \tag{51}$$

where ϕ has been defined in Sec. II C depending on the compact or noncompact nature of the process. Note that the functional relation (51) mirrors the fact the FPT properties of the CTRW are deduced from their DTRW counterpart by means of a time change. In particular, all the geometric dependence is the same in both cases, and the compact or noncompact properties are the same. We define here the walk dimension d_w for the CTRW as the d_w of its DTRW counterpart.

We will focus below on the large-volume limit $N \to \infty$ (and therefore, $\overline{\langle \mathbf{T} \rangle}_T \to \infty$). As seen in Sec. II C, the function $\psi_N(\theta = t/\overline{\langle \mathbf{T} \rangle}_T) = \overline{\langle \mathbf{T} \rangle}_T \phi(t)$ has a well-defined limit in the regime $N \to \infty$. In Laplace space this implies

$$\lim_{N\to\infty} \hat{\phi}(s) = \lim_{N\to\infty} \hat{\psi}_N(\tilde{s} = s\overline{\langle \mathbf{T} \rangle}_T) = \hat{\psi}(\tilde{s}), \tag{52}$$

where $\hat{\psi}(\tilde{s})$ is finite and independent of N. In order to go further, one needs to specify the waiting-time distribution F. Several cases are presented below.

B. Exponential distribution of waiting times

We first focus on the example of exponential waiting-time probability distributions, for which the mean waiting time is finite:

$$F(t) = \alpha \, \exp(-\alpha t). \tag{53}$$

The corresponding Laplace transform reads

$$\hat{F}(s) = \frac{1}{1 + \frac{s}{\alpha}}. \tag{54}$$

Inserting this expression into (51) yields

$$\begin{aligned} \hat{\mathcal{P}}_{TS}(s) &= \hat{P}_{TS}\left[\ln\left(1 + \frac{s}{\alpha}\right)\right]. \\ &= (1 - \Pi_{TS}) + \Pi_{TS}\,\hat{\phi}\left[\ln\left(1 + \frac{s}{\alpha}\right)\right]. \end{aligned} \tag{55}$$

Writing in turn

$$\hat{\phi}\left[\ln\left(1 + \frac{s}{\alpha}\right)\right] = \hat{\psi}_N\left[\overline{\langle \mathbf{T} \rangle}_T \ln\left(1 + \frac{\tilde{s}}{\alpha\overline{\langle \mathbf{T} \rangle}_T}\right)\right] \tag{56}$$

with $\tilde{s} = s\overline{\langle \mathbf{T} \rangle}_T$, one obtains straightforwardly from Eq. (52)

$$\lim_{N\to\infty} \hat{\phi}\left[\ln\left(1 + \frac{s}{\alpha}\right)\right] = \hat{\psi}(\tilde{s}/\alpha), \tag{57}$$

which is finite and independent of N. We then define

$$\eta = \alpha \frac{t}{\overline{\langle \mathbf{T} \rangle}_T}, \tag{58}$$

and denote by Ξ_{TS} the FPT distribution for η, which can be readily deduced from Eqs. (57) and (55) and reads in the large N limit

$$\Xi_{TS}(\eta) = (1 - \Pi_{TS})\,\delta(\eta) + \Pi_{TS}\,\psi(\eta). \tag{59}$$

The FPT distribution for the CTRW model with exponential waiting times is therefore the same function as the FPT distribution of the DTRW in the large N limit. We will show below that this result holds for any waiting-time distribution with finite first moment.

C. Heavy-tailed distribution

In this section we discuss the case of a general distribution of waiting times with a power-law tail (heavy-tailed distribution). We first derive the FPT probability density in the cases of finite and infinite mean waiting times and give the explicit example of Lévy stable laws, which are broad distributions whose Laplace transform has a simple expression.

Let us consider the following example of waiting-time distribution:

$$\begin{cases} t > \left(\frac{\lambda}{\alpha}\right)^{\frac{1}{\alpha}} \; F(t) = \dfrac{\lambda}{t^{1+\alpha}} \quad (\alpha > 0). \\ t < \left(\frac{\lambda}{\alpha}\right)^{\frac{1}{\alpha}} \; F(t) = 0 \end{cases} \tag{60}$$

The Laplace transform of this expression cannot be calculated exactly. Yet, in this work we focus on the large-volume limit of the FPT distribution, which is characterized by the first term of the development of $\hat{F}(s)$ in the neighborhood of $s = 0$, as will be shown later. Let us denote $\Lambda = (\frac{\lambda}{\alpha})^{\frac{1}{\alpha}}$ and write

$$(s\Lambda)^{-\alpha}\,\hat{F}(s) = \alpha \int_{s\Lambda}^{+\infty} \nu^{-(1+\alpha)} e^{-\nu}\, d\nu. \tag{61}$$

1. General heavy-tailed distribution with $\alpha > 1$

We first consider the case $\alpha > 1$, for which the mean waiting time is finite. Equation (61) yields the following expansion:

$$\begin{aligned} \hat{F}(s) = 1 &- \left(\frac{\lambda}{\alpha}\right)^{\frac{1}{\alpha}} \frac{\alpha}{\alpha - 1} s \\ &+ \frac{\lambda}{\alpha(\alpha - 1)}\,\Gamma(2 - \alpha)\, s^{\alpha} + \mathcal{O}(s^2). \end{aligned} \tag{62}$$

Such expansion is very general and applies for an arbitrary asymptotic power-law distributions of parameter $\alpha \leqslant 2$. We now show that in the large N limit all terms s^{β} with $\beta > 1$ are irrelevant to calculate the limit FPT distribution. Let us introduce the rescaled variable:

$$\eta = t/\overline{\langle \mathbf{T} \rangle}_T, \tag{63}$$

and its Laplace conjugate $\tilde{s} = s\overline{\langle \mathbf{T} \rangle}_T$. Using Eq. (62), one obtains from Eqs. (51) and (52), keeping previous notations:

$$\lim_{N\to\infty} \hat{\phi}\{-\ln[\hat{F}(s)]\} = \hat{\psi}\left(\Lambda \frac{\alpha}{\alpha - 1}\tilde{s}\right). \tag{64}$$

Finally, after a further rescaling of the time variable:

$$\eta = \frac{(\alpha - 1)}{\alpha\,\Lambda^{1/\alpha}\,\overline{\langle \mathbf{T} \rangle}_T}\, t, \tag{65}$$

the large-volume FPT distribution of Eq. (59) is recovered:

$$\Xi_{TS}(\eta) = (1 - \Pi_{TS})\,\delta(\eta) + \Pi_{TS}\,\psi(\eta). \tag{66}$$

Noteworthily, the above derivation is valid for *any waiting-time distribution* as soon as its first moment exists. In particular the fact that the waiting-time distribution has an infinite second moment, and therefore is not subject to the central limit theorem, is irrelevant here and leads asymptotically to the same FPT distribution as in the case of a waiting-time distribution with finite second moment.

2. *General heavy-tailed distribution with* $\alpha < 1$

When $\alpha < 1$, the waiting-times distribution has no first moment ("broad" distribution); the expansion of $\hat{F}(s)$ is as follows:

$$\hat{F}(s) = 1 - \frac{\lambda}{\alpha}\,\Gamma(1-\alpha)\,s^{\alpha} + \left(\frac{\lambda}{\alpha}\right)^{\frac{1}{\alpha}} \frac{\alpha}{1-\alpha} s + \mathcal{O}(s^2). \tag{67}$$

The leading term in Eq. (67) is s^{α}, which determines the relevant timescale in the large N limit. We define the rescaled variable by

$$\eta = \frac{t}{\Lambda\,[\Gamma(1-\alpha)\overline{\langle \mathbf{T}\rangle}_T]^{1/\alpha}} \tag{68}$$

and its Laplace conjugate $\tilde{s} = s\,\Lambda\,[\Gamma(1-\alpha)\overline{\langle \mathbf{T}\rangle}_T]^{1/\alpha}$. From Eq. (67), along with Eq. (52),

$$\lim_{N\to\infty} \hat{\phi}\{-\ln[\hat{F}(s)]\} = \hat{\psi}(\tilde{s}^{\alpha}) \equiv \hat{\xi}_{\alpha}(\tilde{s}), \tag{69}$$

where ξ_{α} depends on α and is independent of N. Using Eq. (51), this shows finally that the FPT distribution for the rescaled time η reads, in the large N limit:

$$\Xi_{TS}(\eta) = (1 - \Pi_{TS})\,\delta(\eta) + \Pi_{TS}\,\xi_{\alpha}(\eta). \tag{70}$$

In the compact case, the function ξ_{α} can be obtained by a numerical Laplace inversion. Moreover, in both the noncompact and the compact cases, the large time asymptotics of the FPT distribution can be easily deduced from the small s expansion of the Laplace transform $\hat{\xi}_{\alpha}(\tilde{s})$:

$$\Pi_{TS}\,\hat{\xi}_{\alpha}(\tilde{s}) \underset{\tilde{s}\ll 1}{\sim} -\frac{\langle \mathbf{T}_{TS}\rangle}{\overline{\langle \mathbf{T}\rangle}_T}\,\tilde{s}^{\alpha}. \tag{71}$$

The fact that this lowest-order expansion has the same expression for both exploration types comes from the equality of the first moments of $\hat{\psi}(\tilde{s})$. Thus, we obtain

$$\mathcal{P}_{TS}(t) \sim \frac{\lambda}{t^{1+\alpha}}\,\langle \mathbf{T}_{TS}\rangle. \tag{72}$$

We comment that this power-law decay mirrors the decay of the waiting-time distribution itself (60). This is expected since the first-passage time is a sum of random variables following a broad distribution and should thus be asymptotically distributed according to a stable law with the same decay [20]. Equation (72) provides not only the tail of the FPT PDF but also the prefactor. It is in agreement with Ref. [41], where the case of integer dimensions (Euclidian geometry) had already been derived.

Example of the one-sided Lévy-stable distribution. The Laplace transform $\hat{F}$ of the one-sided Lévy stable distribution of parameter $\alpha < 1$, usually denoted by $f_{\alpha}\,[(t, \cos(\pi\alpha/2), 1, 0]$ [37], reads

$$\hat{F}(s) = \exp(-s^{\alpha}). \tag{73}$$

This is an exact expression. Therefore, Eq. (51) can then be rewritten as

$$\hat{\mathcal{P}}_{TS}(s) = \hat{P}_{TS}(s^{\alpha}) = (1 - \Pi_{TS}) + \Pi_{TS}\,\hat{\phi}(s^{\alpha}). \tag{74}$$

If we introduce the rescaled variable

$$\eta = \frac{t}{\overline{\langle \mathbf{T}\rangle}_T^{1/\alpha}}, \tag{75}$$

and its Laplace conjugate $\tilde{s} = s\,\overline{\langle \mathbf{T}\rangle}_T^{1/\alpha}$, we recover Eq. (70):

$$\Xi_{TS}(\eta) = (1 - \Pi_{TS})\,\delta(\eta) + \Pi_{TS}\,\xi_{\alpha}(\eta). \tag{76}$$

IV. NUMERICAL SIMULATIONS

We now compare the analytical results we obtained in the previous sections with numerical simulations of the FPT distribution, performed on various network models:

(1) Noncompact exploration ($d_w < d_f$): discrete (DTRW) or continuous-time (CTRW) random walks on the 3D cubic lattice and the tridimensional supercritical percolation cluster; two types of "quenched" disorder on the cubic lattice: disordered waiting times at each site (the random-trap model) and disordered transition rates between sites (the random-barrier model).

(2) Marginal exploration ($d_w = d_f$): DTRW and CTRW on the 2D cubic lattice.

(3) Compact exploration ($d_w > d_f$): DTRW and CTRW on deterministic fractals: the Sierpinski gasket and the hierarchical T-tree (see Fig. 1); on random fractals: the tridimensional critical percolation cluster.

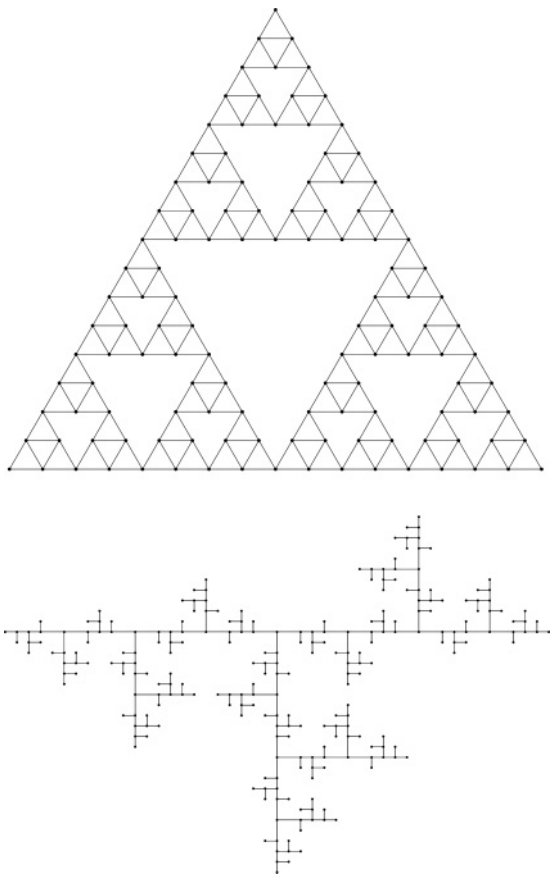

FIG. 1. The fourth-generation Sierpinski gasket and the fifth-generation T-tree.

These models are well known and widely used in statistical physics; for a presentation see, for example, Refs. [19] and [20]. Their diversity illustrates the wide range of applicability of the results of Secs. II and III.

For each model we discuss and justify the applicability of the theory, and a general discussion on the range of validity in time of the theoretical results is proposed in Sec. V. All simulation results have been rescaled to be compared to theoretical expressions (41) and (42) in the case of the DTRW model and to (59), (76), (70), and (66) in the case of the CTRW model. Eventually, let us remind readers that the large-volume assumption (20) that was necessary to compute the results of Secs. II and III does not allow to expect *a priori* the validity of the latter expressions when either the source or the target is close to the network boundaries, or when one of the network spatial extensions is small. We will see that in practice these conditions are very weakly restrictive.

A. Noncompact and marginal exploration

Simulation methods. Euclidian (3D and 2D) DTRW and random-barrier model first-passage distributions have been simulated using the exact enumeration method, which involves the recursive computation of the whole probability field at each time step, using the master equation. The precision that governs the end of the loop was set at 1%. For all the other models we use Monte Carlo simulation. A single network is generated, including the positions of the source and target: In Sec. IV A we merely perform an average over the walks, also called average over the different "thermal histories." The order of magnitude of the number of walks we perform is 100 000 (see legends).

1. 2D and 3D (Euclidean) lattices

When the random walk occurs on a simple and confined (rectangular or parallelepipedic) lattice, the pseudo-Green function H_{ij} is exactly known [42,43]; therefore, the entire expression (41) is explicitly known.

DTRW. Figure 2 shows the results of exact-enumeration simulations. We chose a 1% relative precision. Geometrical settings are detailed in the figure inset legend and are compared to (30); their large variety highlights the robustness of the theoretical result. Indeed, very good agreement is found, even for *a priori* unfavorable geometrical settings: When the source and the target are both close to an edge, or when the confining domain is a stretched parallelepiped.

CTRW. Figure 3 shows the Monte Carlo simulated curves along with the theoretical curves ψ and ξ_α versus the rescaled time variable η, for each of the waiting-time distributions studied in Sec. III. Very good agreement is found in all considered cases. In the case (a) of the exponential distribution ψ (exponential waiting-time distribution and heavy-tailed waiting-time distribution with $\alpha > 1$), several wide-ranged values of α are chosen, and both 3D and 2D lattices are considered. In the case (b) of distribution ξ_α (Lévy-stable and general heavy-tailed distribution with $\alpha < 1$; i.e., having an infinite first moment), the curves are drawn for $\alpha = 0.2$ and 0.8, and for 3D and 2D lattices.

Since the aim of this series of simulated curves is to study the robustness of expressions (59), (76), (70), and (66) with respect to the waiting-time distribution tail rather than to geometrical settings, the shape of the confining domain (e.g., 21-sided cube and 81-sided square) and the positions of the source and of the target ([e.g., in 3D, (12,12,11) and (10,10,10); in 2D, (42,42) and (40,40)] represent simple configurations. Yet, other geometrical settings would give similar results (as the previous study shows; see Fig. 2).

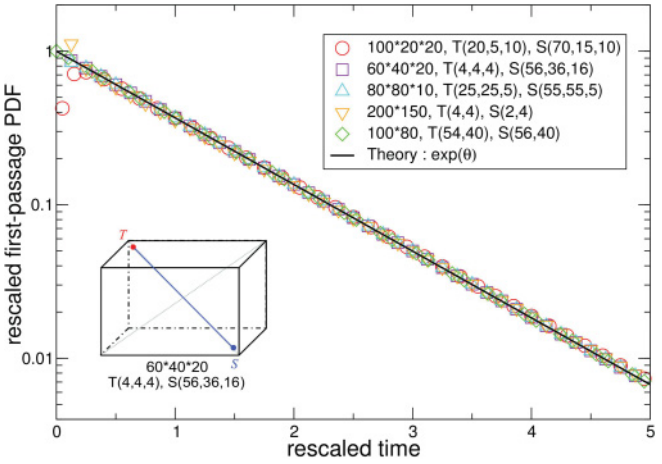

FIG. 2. (Color online) 3D and 2D Euclidean lattices, DTRW. Simulated rescaled first-passage PDFs $Q_{TS}(\theta)/\Pi_{TS}$ [Eq. (40)] obtained by exact enumeration (symbols) are plotted against theoretical distribution $\psi(\theta) = e^{-\theta}$ [Eq. (41a)] (solid line) for several confining domain shapes and source or target positions. Domain dimensions $L_x L_y (L_z)$ and source or target coordinates are indicated in the legend inset. Rescaled time is $\theta = t/\overline{\langle \mathbf{T} \rangle}_T$ [Eq. (39)]. For this type of network, moments $\langle \mathbf{T}_{TS} \rangle$ and $\overline{\langle \mathbf{T} \rangle}_T$ are calculated exactly [42], so the theoretical first-passage distribution depending on t [Eqs. (30) and (31)] is known exactly.

2. 3D supercritical percolation cluster

Random-walk simulations are performed on 3D supercritical bond percolation clusters as an example of noncompact exploration in a disordered environment. Indeed, above criticality (i.e., when the control parameter p is greater than the critical value p_c), the exploration on the infinite percolation cluster is noncompact, and one has $d_w = 2$ and $d_f = 3$. The control parameter value is set to $p = 0.4$ (in the case of bond percolation $p_c \simeq 0.2488$). The clusters are randomly generated, embedded in a cubic lattice; for each of them one source and one target are randomly chosen, and 200 000 walks are performed with this S/T pair.

Figure 4 shows the rescaled first-passage PDF in the DTRW case (a) and for two examples of waiting-time distribution for the CTRW model (b): the exponential and the Lévy-stable distributions. Monte Carlo simulations are plotted against the theoretical prediction ψ (DTRW and exponential CTRW) or ξ_α (Lévy-stable CTRW), for various randomly generated configurations and for different values of parameter α. Very good agreement is found in every case.

3. Random-trap model

The random-trap model (RTM) randomly sets the values of the waiting times of all sites of a network before performing the walks, and these values remain the same during the whole

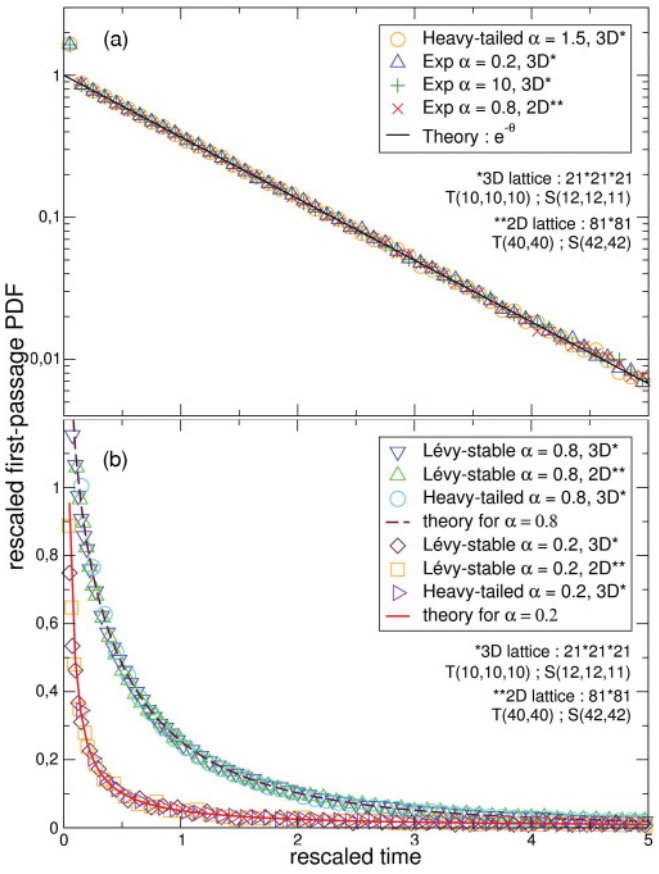

FIG. 3. (Color online) Euclidean lattices, CTRW. Rescaled first-passage PDFs $\Xi(\eta)/\Pi_{TS}$ performed by simulation (symbols) are compared to the corresponding theoretical functions $\psi(\eta)$ or $\xi_\alpha(\eta)$ (solid lines) [Eqs. (59), (76), (70), and (66)]. The chosen lattice shapes, along with the source and target coordinates, are indicated in the legend insets. Numerical curves are obtained by Monte Carlo methods; 100 000 walks are performed. The first-passage moments $\langle \mathbf{T}_{TS} \rangle$ and $\overline{\langle \mathbf{T} \rangle}_T$ are calculated exactly [42]. Thus, the theoretical first-passage distributions depending on t are known exactly in each case. (a) Exponential waiting-time distribution $[F(t) = \alpha \exp(-\alpha t)]$ and heavy-tailed waiting-time distribution $[F(t) = 1/t^{1+\alpha}$ for $t > 1/\alpha^{1/\alpha}]$ with $\alpha > 1$. Respective rescaled times are $\eta = \alpha t/\overline{\langle \mathbf{T} \rangle}_T$ and $\eta = (\alpha - 1)t/\alpha^{1-1/\alpha}\overline{\langle \mathbf{T} \rangle}_T$ [Eqs. (58) and (65)]. (b) Lévy-stable waiting-time distribution $[F(t) = f_\alpha(t, \cos(\pi\alpha/2), 1, 0)]$ and heavy-tailed waiting-time distribution with $\alpha < 1$. Values $\alpha = 0.8$ and $\alpha = 0.2$ are chosen. Respective rescaled times are $\eta = t/\overline{\langle \mathbf{T} \rangle}_T^{1/\alpha}$ and $\eta = [\alpha/\Gamma(1-\alpha)\overline{\langle \mathbf{T} \rangle}_T]^{1/\alpha} t$ [Eqs. (75) and (68)].

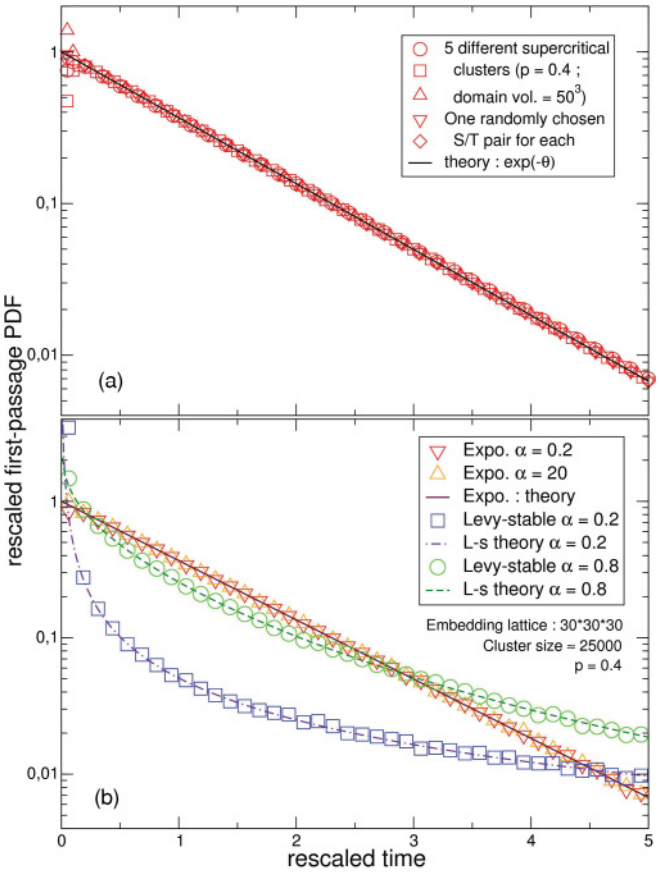

FIG. 4. (Color online) 3D supercritical percolation (control parameter $p = 0.4$). Each of the plotted rescaled first-passage distributions (symbols) corresponds to one randomly generated cluster; the source and the target position are randomly chosen, and calculations are obtained by Monte Carlo methods, performing 200 000 walks. Quantities $\langle \mathbf{T}_{TS} \rangle$ and $\overline{\langle \mathbf{T} \rangle}_T$, that are necessary to compute the rescaled time and the prefactor Π_{TS} are computed numerically. (a) DTRW: five clusters embedded in 50^3 domains are generated; numerical PDFs are drawn along with the theoretical (solid line) curve $\psi(\theta)$ [see Eq. (41)] where $\theta = t/\overline{\langle \mathbf{T} \rangle}_T$. (b) CTRW: four clusters embedded in 30^3 domains are generated (their volume are approximatively $N \simeq 25\,000$); simulated curves are drawn for both the exponential and the Lévy-stable waiting-time distribution, in each case for two very different values of α. Theoretical curves $\psi(\eta)$ and $\xi_\alpha(\eta)$ [obtained by numerically inverse-Laplace transforming (74)] are drawn in solid or dashed lines for comparison [see (59) and (76)]. Rescaled time variables are $\eta = \alpha t/\overline{\langle \mathbf{T} \rangle}_T$ [exponential, (58)] and $\eta = t/\overline{\langle \mathbf{T} \rangle}_T^{1/\alpha}$ [Lévy stable, (75)].

Monte Carlo calculation; therefore, contrary to the CTRW, it belongs to the class of quenched (frozen) disorder models. We used 3D Euclidian lattices, for which the dimensions remain $d_f = 3$ and $d_w = 2$. Note that strictly speaking, the RTM cannot be described in the framework developed in this paper, which deals with random walks defined by transition probabilities w_{ji}: Here the waiting time τ_i of each site is a fixed (nonrandom) quantity. The model is, however, well approximated by a random walk with transition probabilities $w_{ii} = 1 - 1/\tau_i$ and $w_{ji} = 1/(2d\tau_i)$ for j nearest neighbor of i, for which our method applies. We will check numerically that this approximation holds only when the first moment of τ_i is finite.

We consider here the following heavy-tailed waiting-time distribution:

$$\begin{cases} \tau > 1 & \rho(\tau) = \dfrac{\alpha}{\tau^{1+\alpha}} \\ \tau < 1 & \rho(\tau) = 0. \end{cases}$$

Figure 5 shows the rescaled first-passage PDF resulting from Monte Carlo simulations for diverse lattice shapes, source or target positions, and values of parameter α (in the interval $[0, 2]$), as is indicated in the figure legend and inset. Once again, we stress the wide-range validity of the theoretical results when

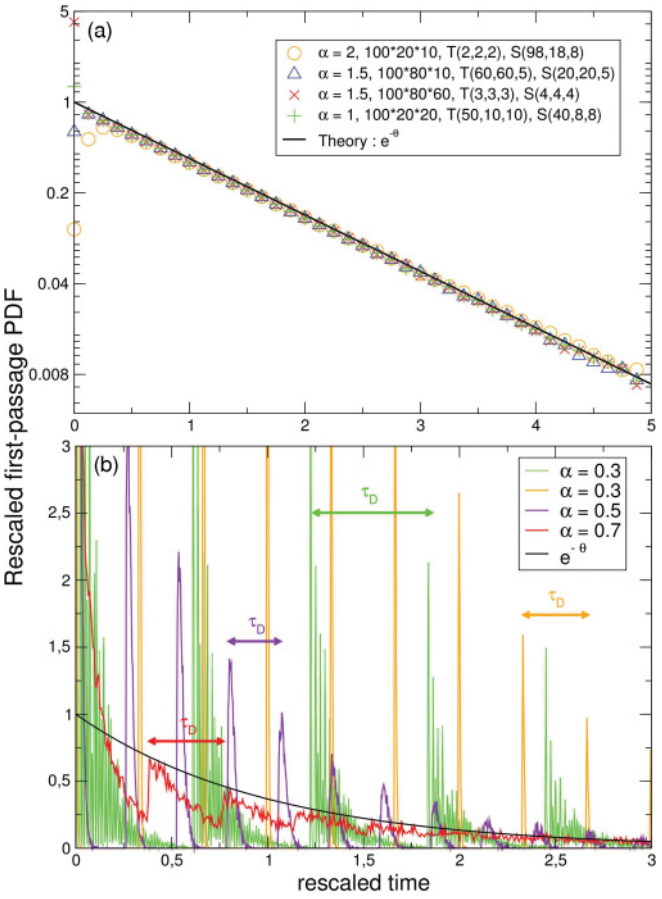

FIG. 5. (Color online) Random-trap model for a 3D lattice. Waiting times are associated to each site of the lattice, randomly derived from the distribution $\rho(\tau) = \frac{\alpha}{\tau^{1+\alpha}}$ for $\tau > 1$. These times do not vary during the whole Monte Carlo calculation (frozen disorder). 200 000 random walks are performed. (a) Simulated rescaled first-passage PDF (symbols) compared to the theoretical distribution $\psi(\theta)$ given by Eq. (41) (solid line), for various embedding lattice shapes, coordinates of the source and target, and $\alpha > 1$ values (see legend inset). These settings are chosen for their diversity. $\langle \mathbf{T}_{TS} \rangle$ and $\overline{\langle \mathbf{T} \rangle}_T$ are calculated numerically, $\theta = t/\overline{\langle \mathbf{T} \rangle}_T$ [Eq. (39)]. (b) Examples of first-passage PDF when $\alpha < 1$. In the four cases, calculations were made using a 20^3 domain, a target at (5,7,9), and a source at (12,13,12). The waiting time τ_D of the deepest trap is represented in each case; it corresponds to the pseudoperiod of the oscillations.

$\alpha > 1$ with respect to geometrical settings (see inset of Fig. 5), which notably differ from the ideal large-volume assumption.

Figure 5(b) shows that the agreement between the theoretical prediction and numerical simulations is good only for $\alpha > 1$, while a significant deviation is observed when $\alpha < 1$. Actually, when $\alpha < 1$, the random-trap model cannot be satisfactorily approximated by a discrete-time random walk with transition probabilities, so that the general theory of previous sections does not apply. Qualitatively, for α small, the waiting-time distribution in the network becomes very inhomogeneous, and the FPT can be dominated by the waiting time in the deepest trap D, which is a deterministic quantity for the random-walk process. An estimate of this longest waiting time denoted τ_D can be obtained following Ref. [20]. It is given by

$$N \int_{\tau_D}^{\infty} \rho(\tau) d\tau \approx 1, \tag{77}$$

which, when using the distribution ($\rho(\tau > 1) = \frac{\alpha}{\tau^{1+\alpha}}$), leads to

$$\tau_D \gtrsim N^{1/\alpha}. \tag{78}$$

Hence, for $\alpha < 1$ the longest waiting time τ_D has the same order of magnitude as the sum of all waiting times $\sum_{k=0}^{N} \tau_k$, and one can expect that the FPT is controlled by τ_D. Since this quantity is deterministic, the analysis presented in this paper does not apply in this case.

Figure 5 shows that when $\alpha < 1$, pseudoperiodic oscillations appear on the FPT distribution curve, and their amplitudes grow when α decreases. It is possible to give an interpretation of such a phenomenon. Numerical simulations show that the pseudoperiod is roughly equal to the deepest trap waiting time, which suggests that these oscillations correspond to the successive "falls" of the random walker in the deepest trap of the domain.

4. Random-barrier model

The random-barrier model (RBM) is another very useful example of model of transport in an environment with frozen disorder. Whereas the random-trap model assigns waiting-time values to all sites of the network, the RBM assigns frozen random transition frequencies to the links between sites. We consider here the following heavy-tailed distribution of jump frequency (using $\Gamma_0 = 1$):

$$\begin{cases} \Gamma < \Gamma_0 & \rho(\Gamma) = \frac{\alpha}{\Gamma} \left(\frac{\Gamma}{\Gamma_0}\right)^{\alpha} \\ \Gamma > \Gamma_0 & \rho(\Gamma) = 0 \end{cases}, \quad \text{with} \quad 0 < \alpha < 1,$$

which correspond to exponentially distributed energy barriers [44]. It can be shown that for this model one has $d_f = 3$ and $d_w = 2$ provided that $\alpha > 1/6$ [20]. Figure 6(a) shows an excellent agreement between simulations and the theoretical prediction (41), even for source and target positions close to the domain boundary, for α values ranging from 1/6 to 1.

Interpretation of the threshold $\alpha = 1/6$. Figure 6(b) displays two examples of simulated FPT distributions when $\alpha < 1/6$, which no longer agree with (41). This threshold can be understood as follows. Let $\Gamma_{i,k}$ ($k = 1, \ldots, 2d$) be the transition frequencies from site i to its $2d$ neighbors. The distribution of the waiting time on site i is given by the exponential law: $p_i(t) = \exp[-(\sum_{k=1}^{2d} \Gamma_{i,k})t]$. Therefore, the mean waiting time is

$$\langle t \rangle_i = \frac{1}{\sum_{k=1}^{2d} \Gamma_{i,k}}. \tag{79}$$

Now, let us evaluate the distribution over disorder of this mean waiting time. Using the latter result, $P(\langle t \rangle_i > \tau_0) = P(\sum_{k=1}^{2d} \Gamma_{i,k} < \frac{1}{\tau_0})$. A necessary condition to fulfill the inequality $\sum_{k=1}^{2d} \Gamma_{i,k} < \frac{1}{\tau_0}$ is that every frequency is lower than $1/\tau_0$. Therefore,

$$P(\langle t \rangle_i > \tau_0) \simeq \left[\int_0^{1/\tau_0} \rho(\Gamma) d\Gamma \right]^{2d} \simeq (\Gamma_0 \tau_0)^{-2d\alpha}, \tag{80}$$

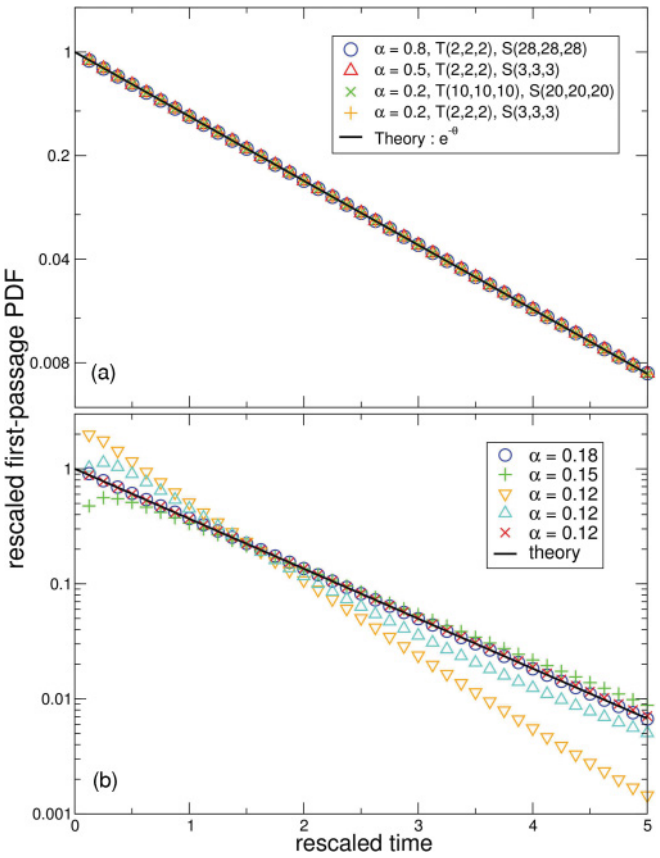

FIG. 6. (Color online) Random-barrier model on a cubic ($N = 30^3$) lattice: Rescaled first-passage PDFs are calculated using the exact-enumeration method (symbols) and are compared to the theoretical function $\psi(\theta)$ (41) (solid line) for various positions of the source and the target and for various α value settings. All rescaling parameters ($\langle \mathbf{T}_{TS} \rangle$ and $\overline{\langle \mathbf{T} \rangle}_T$) are numerically calculated by exact enumeration. (a) Parameter α is greater than the critical value 1/6. (b) Crossing the α threshold: $\alpha > 1/6$ (one realization) and $\alpha < 1/6$ (four realizations).

from which one easily deduces the distribution of the mean waiting times:

$$p(\langle t \rangle_i) = \frac{2d\alpha}{\Gamma_0^{2d\alpha} \langle t \rangle_i^{2d\alpha+1}}. \tag{81}$$

Distribution (81) admits a finite first moment if

$$\alpha > 1/2d. \tag{82}$$

When this condition (82) is not fulfilled, the FPT is controlled by the longest mean waiting time. In this case the propagator does not satisfy the standard scaling of Eq. (25), and the hypothesis of Eq. (23) is not verified. Hence Eq. (41) does not apply, as confirmed in Fig. 6(b).

Remark. Unlike the random-trap model, oscillations do not appear when $\alpha < \alpha_{\text{crit}}$ in the random-barrier model. This can be explained by the difference between both models, namely, between a trap and a barrier. Indeed, in the RTM case, the walker, once having left the deepest trap, is likely to fall in it repeatedly. In the RBM case, however, once the walker has left the site with longest waiting time, it will most probably not reach this site anymore, because of the high barriers that surround it.

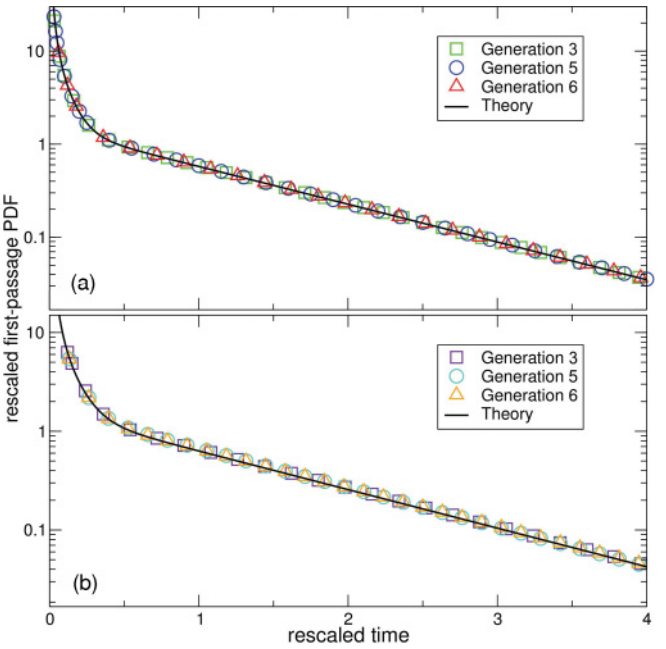

FIG. 7. (Color online) Deterministic fractals, DTRW. Rescaled first-passage densities $Q_{TS}(\theta)$ [symbols, see Eq. (40)] obtained by exact enumeration are drawn versus the theoretical prediction $\psi(\theta)$ [solid lines, see Eq. (42b)] for different generations (see insets). The target is fixed and the curves are averaged over all the sources of the network to fulfill the isotropy hypothesis of the propagator (in other words, for each generation, the plotted points result from an average over the rescaled PDFs of the walks starting from every site of the network, and ending at the chosen target). The quantity $\overline{\langle \mathbf{T} \rangle}_T$ that is needed to rescale the results is calculated exactly [45,46]. (a) Sierpinki gasket; the target is set at the apex. (b) T-graph; the target is set at the central node.

B. Compact exploration

We use exact enumeration for DTRW on deterministic fractals and Monte Carlo calculation in the other cases. Whereas in the previous section each FPT distribution was drawn for a single source or target pair, the results presented in this section are averaged over the source position (Sierpinski gasket and T-tree) or over the positions of both the source and the target (critical percolation clusters). This choice is commented on in Sec. IV B 3. Let us already notice that in the Monte Carlo cases, the algorithm hierarchy is the as follows: First, we perform from 500 to 5000 walks for each source or target pair, depending on the network; then, we apply the average over the sources or the pairs. In order to get results that do not depend on the arbitrarily chosen number of walks per pair, we need both types of averages to commute.

1. *Deterministic fractals: The Sierpinski gasket and the T-graph*

Both networks are presented in Fig. 1.

DTRW. Figure 7 shows an excellent agreement between numerical and theoretical results (42) *on the entire time range* (see Sec. V) for both networks. We stress that this remains true

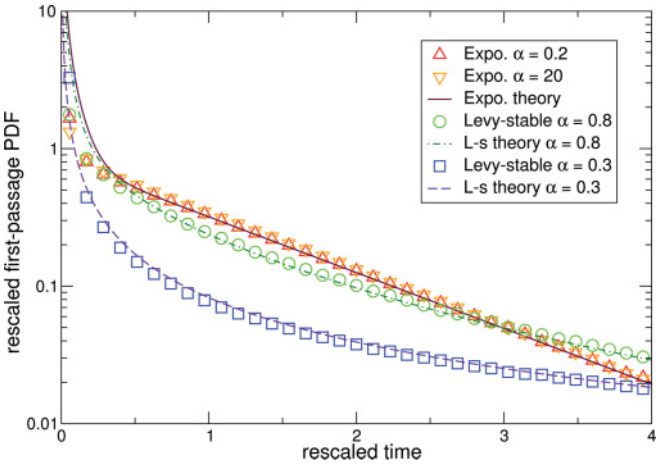

FIG. 8. (Color online) Sierpinski gasket, CTRW. Rescaled first-passage densities $\xi_{TS}(\eta)$ (symbols) obtained by Monte Carlo calculation are drawn versus the theoretical predictions (solid lines). Exponential waiting-time distribution: $\psi(\eta)$ with $\eta = \alpha t/\overline{\langle \mathbf{T} \rangle}_T$ [Eq. (59)]. Lévy-stable waiting-time distribution: $\xi_\alpha(\eta)$ with $\eta = t/\overline{\langle \mathbf{T} \rangle}_T^{1/\alpha}$ [Eq. (76)]. The values of parameter α are chosen to be representative of the range of possibilities. The network generation is 5, the target is set at the apex, and the results are averaged over the sources. 5000 walks are performed for each source. The quantity $\overline{\langle \mathbf{T} \rangle}_T$ is known exactly [45].

even for very small networks (respectively, 42 and 28 sites for the third-generation Sierpinski gasket and T-graph). Note that in the case of deterministic fractals, the first moments of the MFPT and the GMFPT can be calculated analytically in some cases [45–48], which yields, following (37), a fully explicit determination of the FPT distribution.

CTRW. Continuous-time random-walk simulations performed on the Sierpinski gasket for the exponential and the Lévy-stable waiting-time distribution are shown in Fig. 8. Very good agreement with theory [Eqs. (59) and (76)] is found. We remind readers here that d_w has by definition the same value as in the case of a DTRW. Although the results are not presented here, this agreement was also confirmed by simulations on the T-graph.

2. The 3D critical percolation cluster

Tridimensionnal critical bond percolation is chosen as an example of random fractal. Each curve of Fig. 9 corresponds to the random generation of a single percolation cluster, but then to an average over source or target pairs. They are results of Monte Carlo simulations for the DTRW and the CTRW with two examples of waiting-time distributions [exponential and Lévy-stable) and compared to the theoretical prediction (42)]. Good agreement with theoretical results (42), (59), and (76) is found. A slight discrepancy is observed [see Fig. 9(b)] for the heavy-tailed CTRW with $\alpha = 0.4$: the more α is low, the more inhomogeneous the system will be, thus affecting the assumptions made in the compact case (see Sec. IV B 3). Note that we used the critical dimensions corresponding to chemical distances [19]: $d_f = 1.84$ and $d_w = 2.82$.

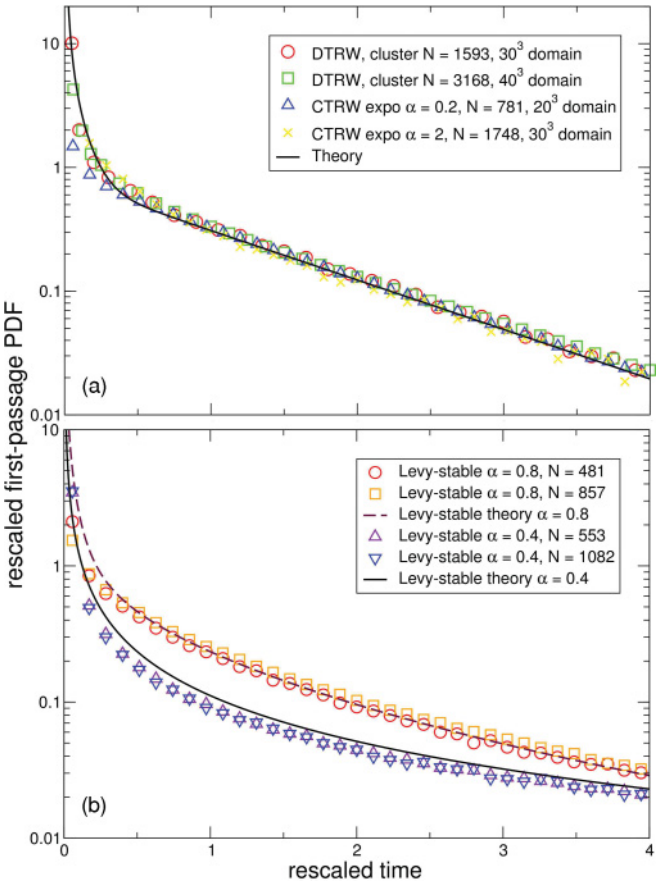

FIG. 9. (Color online) 3D critical bond percolation (control parameter $p = 0.248812$). Each of the plotted rescaled FP PDFs (symbols) corresponds to one randomly generated cluster and an average over 100 source or target couples and 2000 walks for each couple; calculations are performed by Monte Carlo methods. $\overline{\langle \mathbf{T} \rangle}_T$ (used to compute the rescaled time) is computed numerically. We use dimensions corresponding to chemical distance: $d_f = 1.84$ and $d_w = 2.82$. (a) DTRW (two clusters) corresponding to Eq. (42b) with $\theta = t/\overline{\langle \mathbf{T} \rangle}_T$; and exponential waiting-time CTRWs for two values of α (0.2 and 2, see legend inset) corresponding to Eq. (59) with $\eta = \alpha t/\overline{\langle \mathbf{T} \rangle}_T$. (b) Lévy-stable waiting-time CTRW for two values of α: 0.4 and 0.8, with two simulated clusters for each. See Eq. (76); the rescaled time is $\eta = t/\overline{\langle \mathbf{T} \rangle}_T^{1/\alpha}$.

3. Averaged and nonaveraged results

The results presented in this section, i.e., those displayed in Figs. 7, 8, and 9, are averaged results. Actually, nonaveraged curves (single source or target pair and disorder realization) obtained on these networks (deterministic fractal networks and critical percolation cluster) show, in general, much larger discrepancies with the theoretical results than in the noncompact exploration cases that have been presented previously. Figure 10 illustrates this deviation: Each of the three figures a, b, and c corresponds to a realization of a percolation cluster embedded in a 30^3 cube, for different values of the control parameter p (the bond existence probability). Critical percolation, $p = p_c = 0.28814$ (a), is compact; supercritical percolation ($p = 0.3$ and $p = 0.4$, b and c) is noncompact. In each case a random sample of 12 source or target pairs is chosen and the FPT densities are drawn. Panel d shows a

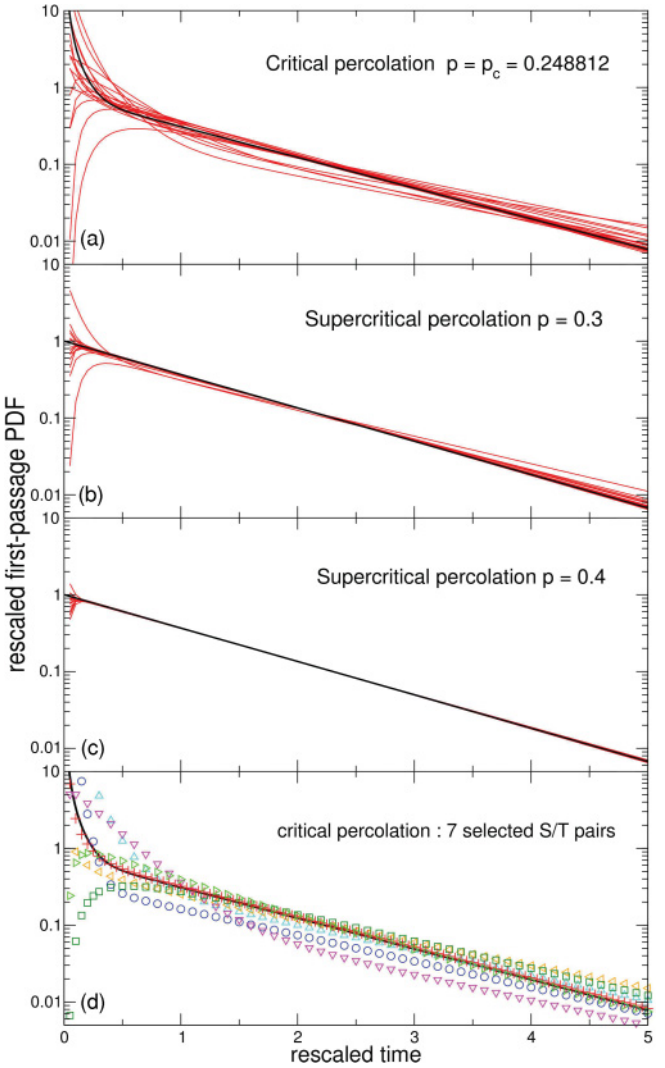

FIG. 10. (Color online) 3D critical percolation cluster, nonaveraged first-passage densities (each curve corresponds to one source or target pair). (a–c) FP PDFs of 12 randomly chosen source or target pairs (red curves) compared to the theoretical prediction [(42b), black curves], for three different values of the percolation control parameter p: $p = p_c = 0.28814$, $p = 0.3$, and $p = 0.4$. The two latter values correspond to noncompact cases. (d) Seven particularly deviant source or target cases.

sample of particularly deviant source or target cases in critical percolation. The Sierpinski and the T-tree networks show the same kind of deviation.

Let us now discuss this deviation, which appears only in compact exploration cases in the examples that we have studied. Actually, as we put forward in Sec. II, we needed to make use of the O'Shaughnessy-Procaccia propagator to evaluate the pseudo-Green functions and the moments of the compact distribution. As is detailed in Appendix D, the O'Shaughnessy-Procaccia propagator is a function of r^{d_w}/t only (up to a normalization factor), which comes from the fact that the O'Shaughnessy-Procaccia equation actually implicitly involves an average over shells of radius r. In other words, in the compact case, the theoretical results involve an isotropic approximation. This approximation is not needed in the case of noncompact exploration. This could explain the striking difference found between anisotropic models depending on their compact (Sierpinski gasket) or noncompact nature (RTM). In the case of compact exploration, one needs to restore the isotropy encompassed by the O'Shaughnessy-Procaccia propagator, that is, the meaning of the averaged we perform in Figs. 7–9. The observed deviation in the case of compact exploration suggests that the FPT distribution is not a self-averaging quantity in the examples that we have examined. Eventually, as mentioned above, we note that the order in which spatial averages and ensemble averages are taken does not change the results as was checked numerically.

V. TIME-RANGE VALIDITY OF THE THEORETICAL RESULTS

As one focuses on the short rescaled-time regime, one can notice discrepancies between numerical and theoretical results, in both compact and noncompact cases (see Fig. 11). To try and understand the behavior of the FPT distribution function in the short rescaled-time regime, let us start by considering the instructive example of normal diffusion in one dimension.

Unidimensional problem. We consider a Brownian particle of diffusion coefficient K that starts from position $r > 0$. The target is at position $x = 0$ and a reflecting wall is at position $x = R$. The exact expression for the Laplace transform of the FPT distribution probability is given by [49]

$$\hat{P}_{TS}(s) = \cosh\left(\sqrt{\frac{s}{K}}r\right) - \tanh\left(\sqrt{\frac{s}{K}}R\right)\sinh\left(\sqrt{\frac{s}{K}}r\right). \tag{83}$$

We saw in Sec. II that the natural time variable of the problem is the rescaled time $\theta = t/\overline{\langle \mathbf{T}\rangle}_T$. We thus introduce the Laplace variable u, associated to the time θ, and defined by

$$u = s\,\overline{\langle \mathbf{T}\rangle}_T, \tag{84}$$

where

$$\overline{\langle \mathbf{T}\rangle}_T = \frac{R^2}{3K}. \tag{85}$$

Relation (85) is straightforwardly deduced from the results of Ref. [49]. The Laplace transform $\hat{Q}_{TS}$ of the FPT distribution Q_{TS} for θ reads

$$\begin{aligned}\hat{Q}_{TS}(u) &= \hat{P}_{TS}(u/\overline{\langle \mathbf{T}\rangle}_T)\\ &= \cosh\left(\sqrt{3u}\,\frac{r}{R}\right) - \tanh(\sqrt{3u})\sinh\left(\sqrt{3u}\,\frac{r}{R}\right).\end{aligned} \tag{86}$$

Let us now discuss the meaning of the large-volume limit approximation, which our results rely on from Sec. II B 2 onward. As we will show precisely next, that limit unsurprisingly translates into expanding (86) for $\sqrt{3u}\,\frac{r}{R} \ll 1$. Replacing u by its expression $s\overline{\langle \mathbf{T}\rangle}_T$ then yields the following restriction for s:

$$s \ll s_c = \frac{K}{r^2} = \frac{1}{3\overline{\langle \mathbf{T}\rangle}_T}\left(\frac{R}{r}\right)^2, \tag{87}$$

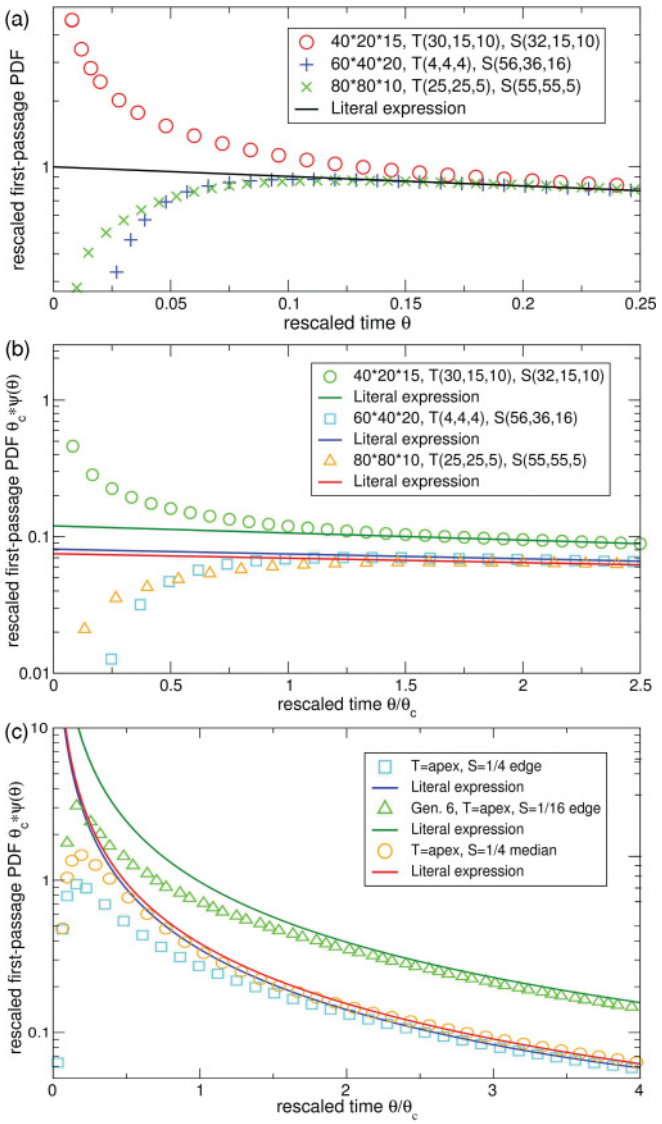

FIG. 11. (Color online) Discrepancy in the short-time regime. (a) Curves are drawn against $\theta = t/\overline{\langle \mathbf{T} \rangle}_T$. This temporal variable corresponds to the "natural" timescale of the first-passage process, i.e., of the first-passage density decay. Example of the 3D Euclidean lattice for various settings (see legend inset). (b, c) Curves are drawn against the variable θ/θ_c, where the meaning of θ_c is discussed in Sec. V: (b) example of noncompact exploration (the 3D Euclidean lattice, characteristics in the legend inset) corresponding to Eq. (109); (c) example of compact exploration (the Sierpinski gasket, characteristics detailed in the legend inset) corresponding to Eq. (101).

which implies for the time t:

$$t \gg t_c = \frac{r^2}{K} = 3\overline{\langle \mathbf{T} \rangle}_T \left(\frac{r}{R}\right)^2, \tag{88}$$

and for θ:

$$\theta \gg \theta_c = 3\frac{r^2}{R^2}. \tag{89}$$

Quite surprisingly, the time regime (88) is independent of the system size R. This implies that the range of validity of the large-volume limit is very wide. In particular, provided that (89) holds, the large-volume limit can be valid even for $\theta \ll 1$. We need to verify that the relations above, applied to expression (86), correspond to the results of Sec. II. Expanding (86) for $\sqrt{3u}\frac{r}{R} \ll 1$ yields

$$\hat{Q}_{TS}^{\infty}(u) \sim 1 - \frac{r}{R}\sqrt{\frac{u}{K}} \tanh\left(\sqrt{\frac{u}{K}}\right), \tag{90}$$

which is naturally equal to $\hat{P}_{TS}(u/\overline{\langle \mathbf{T} \rangle}_T)$, where $\hat{P}_{TS}$ is given by (32), with $d_w = 2$ and $d_f = 1$.

In order to fully encompass the meaning of the large-volume approximation, let us now compute the 1D problem, starting from the exact distribution Laplace transform (86), and following two different ways: on the one hand, we will calculate the exact FPT PDF by Laplace inversion of Eq. (86), and then apply the large-volume approximation to the result. On the other hand, we first apply the large-volume approximation to the Laplace transform, yielding Eq. (90), and then we apply the Bromwich formula to the latter expression.

In the first case, as function (86) has simple poles $u_k = -\frac{1}{3}(k+\frac{1}{2})^2\pi^2$, $k \in \mathbb{N}$, we get the following exact expression:

$$Q_{TS}(\theta) = \sum_{k=0}^{\infty} \frac{\pi}{3}\left(k+\frac{1}{2}\right) \sin\left[\frac{r}{R}\left(k+\frac{1}{2}\right)\pi\right] \times \exp\left[-\frac{1}{3}\left(k+\frac{1}{2}\right)^2 \pi^2 \theta\right]. \tag{91}$$

Now, if one simply applies the approximation

$$\sin\left[\frac{r}{R}\left(k+\frac{1}{2}\right)\pi\right] \xrightarrow[\sqrt{3u}\frac{r}{R} \ll 1]{} \left(k+\frac{1}{2}\right)\frac{\pi r}{R} \tag{92}$$

to each of the terms of (91), we find

$$Q_{TS}^{\infty}(\theta) = \sum_{k=0}^{\infty} \frac{r\pi^2}{3R}\left(k+\frac{1}{2}\right)^2 e^{\left(-\frac{1}{3}(k+\frac{1}{2})^2\pi^2\theta\right)}, \tag{93}$$

which is exactly the formula (42) with $d_w = 2$ and $d_f = 1$. The previous calculation highlights a crucial difficulty that has been introduced in Sec. II C: One should be careful when applying the limit (92) to the infinite sum (91), because the convergence is only pointwise and not uniform over $[0, +\infty[$. As a consequence, the resulting function (93) is not normalized, as mentioned in Sec. II C. That is why in the compact case, it is necessary to specify that the first-passage probability distribution is equal only to (93) in the time regime given by (88).

Let us now proceed and apply the Bromwich formula to the large-volume-approximated $\hat{Q}_{TS}$ (90). Once again (see Sec. II C), we stress that expression (90) is not a Laplace transform, since its limit when $u \to \infty$ is not zero. Nevertheless, applying the Bromwich formula, we get

$$Q_{TS}^{\infty}(\theta) = \sum_{k=0}^{\infty} \frac{r\pi^2}{3R}\left(k+\frac{1}{2}\right)^2 e^{\left[-\frac{1}{3}(k+\frac{1}{2})^2\pi^2\theta\right]}, \tag{94}$$

which is equal to (93). The latter result enlightens the meaning of all the large-volume approximations that have been necessary throughout our calculation in Sec. II. It validates the fact that we deduce the large-volume temporal FPT PDF from a large-volume limit of its moments.

Compact exploration. This analysis of the range of validity of the large-volume limit can be extended to diffusions described by the O'Shaughnessy-Procaccia transport equation in the case of compact exploration. The general exact expression for the Laplace transform of the FPT distribution probability reads

$$\hat{P}_{TS}(s) = d_w^{\nu-1}\left(\frac{s\,r^{d_w}}{K}\right)^{(1-\nu)/2}\Gamma(\nu) \times \frac{1}{I_{-\nu}[x(R,s)]}\{I_{\nu-1}[x(r,s)]I_{-\nu}[x(R,s)] - I_{1-\nu}[x(r,s)]I_{\nu}[x(R,s)]\}, \tag{95}$$

where

$$x(r,s) = \frac{2}{d_w}\sqrt{\frac{r^{d_w}\,s}{K}}. \tag{96}$$

The exact expression for the Laplace transform $\hat{Q}_{TS}$ is then

$$\hat{Q}_{TS}(u) = \left[\left(\frac{r}{R}\right)^{d_w}\frac{d_w^2-d_f^2}{2d_w d_f}\,u\right]^{(1-\nu)/2} \times \frac{1}{I_{-\nu}\,[Y(u)]}\,\{I_{\nu-1}\,[X(u)]\,I_{-\nu}\,[Y(u)] - I_{1-\nu}\,[X(u)]\,I_{\nu}\,[Y(u)]\}\,, \tag{97}$$

with

$$X(u) = \sqrt{\left(\frac{r}{R}\right)^{d_w}\frac{2(d_w^2-d_f^2)}{d_w\,d_f}\,u} \tag{98}$$

and

$$Y(u) = \sqrt{\frac{2\left(d_w^2-d_f^2\right)}{d_w\,d_f}\,u}. \tag{99}$$

As for the particular case of one-dimensional normal diffusion, the asymptotic large-volume behavior of $\hat{Q}_{TS}$ is obtained by expanding (97) for $R \to \infty$ at fixed u, i.e., for $X \ll 1$. We get

$$\hat{Q}_{TS}(u) \sim 1 - \left(\frac{r}{R}\right)^{d_w-d_f}\left(\frac{Y(u)}{2}\right)^{2(1-\nu)} \times \frac{\Gamma(\nu)}{\Gamma(2-\nu)}\,\frac{I_{\nu}\,[Y(u)]}{I_{-\nu}\,[(Y(u)]}, \tag{100}$$

where Y is given by (99). Let us remark that (100) is naturally equal to $\hat{P}_{TS}(u/\overline{\langle \mathbf{T}\rangle}_T)$, where $\hat{P}_{TS}$ is given by (32). The expansion for $X \ll 1$ reduces the regime of validity of (100) to $s \ll s_c = \frac{d_w^2}{4}\frac{K}{r^{d_w}}$, i.e., $t \gg t_c = \frac{4}{d_w^2}\frac{r^{d_w}}{K}$, or

$$\theta \gg \theta_c = \frac{2\left(d_w^2-d_f^2\right)}{d_w d_f}\left(\frac{r}{R}\right)^{d_w}. \tag{101}$$

The evolution of the FPT distribution probability versus the rescaled variable θ/θ_c is plotted in Fig. 11, which confirms this result. Again, as in the 1D case, we stress that the timescale t_c above which the large-volume limit holds is independent of the system size, which makes this asymptotics very robust in practice.

Noncompact exploration. We now turn to the case of noncompact exploration. Using the O'Shaughnessy-Procaccia transport equation, the expression for the Laplace transform of the FPT density reads

$$\hat{P}_{TS}(s) = \left(\frac{a}{r}\right)^{(d_f-d_w)/2} \times \frac{I_{\nu-1}[x(r,s)]I_{-\nu}[x(R,s)] - I_{1-\nu}[x(r,s)]I_{\nu}[x(R,s)]}{I_{\nu-1}[x(a,s)]I_{-\nu}[x(R,s)] - I_{1-\nu}[x(a,s)]I_{\nu}[x(R,s)]}, \tag{102}$$

where x is given by (96), and where a is a characteristic microscopic length scale of the order of the step size. As for the case of compact exploration, the natural time variable to consider is $\theta = t/\overline{\langle \mathrm{T}\rangle}_T$, where $\overline{\langle \mathrm{T}\rangle}_T$ is now given by

$$\overline{\langle \mathbf{T}\rangle}_T = \frac{a^{d_w-d_f}R^{d_f}}{K d_f(d_f-d_w)}. \tag{103}$$

The corresponding Laplace variable is $u = s\overline{\langle \mathbf{T}\rangle}_T$ and the Laplace transform $\hat{Q}_{TS}$ satisfies

$$\hat{Q}_{TS}(u) = \left(\frac{a}{r}\right)^{(d_f-d_w)/2} \times \frac{I_{\nu-1}[\tilde{X}(u)]I_{-\nu}[\tilde{Y}(u)] - I_{1-\nu}[\tilde{X}(u)]I_{\nu}[\tilde{Y}(u)]}{I_{\nu-1}[\tilde{Z}(u])I_{-\nu}[\tilde{Y}(u)] - I_{1-\nu}[\tilde{Z}(u)]I_{\nu}[\tilde{Y}(u)]}, \tag{104}$$

with

$$\tilde{X}(u) = \frac{2}{d_w}\sqrt{d_f(d_f-d_w)\left(\frac{a}{R}\right)^{d_f}\left(\frac{r}{a}\right)^{d_w}u}, \tag{105}$$

$$\tilde{Y}(u) = \frac{2}{d_w}\sqrt{d_f(d_f-d_w)\left(\frac{a}{R}\right)^{d_f-d_w}u}, \tag{106}$$

and

$$\tilde{Z}(u) = \frac{2}{d_w}\sqrt{d_f(d_f-d_w)\left(\frac{a}{R}\right)^{d_f}u}. \tag{107}$$

To obtain the expression of $\hat{Q}_{TS}(u)$ when $R \to \infty$ at fixed u, one expands (104) for $\tilde{X}(u) \ll 1$, $\tilde{Y}(u) \ll 1$, and $\tilde{Z}(u) \ll 1$, which imply, respectively, that $s \ll s_c = \frac{d_w^2}{4}\frac{K}{r^{d_w}}$, $s \ll S_c = \frac{d_w^2}{4}\frac{K}{R^{d_w}}$, and $s \ll \frac{d_w^2}{4}\frac{K}{a^{d_w}}$. Since $a < r < R$, the most constraining condition on s is $s \ll \tilde{s}_c$, which translates into

$$t \gg T_c = \frac{4}{d_w^2}\frac{R^{d_w}}{K} \tag{108}$$

and

$$\theta \gg \Theta_c = \frac{4d_f(d_f-d_w)}{d_w^2}\left(\frac{R}{a}\right)^{d_w-d_f}. \tag{109}$$

The large-volume limit expression of $\hat{Q}_{TS}$ is

$$\hat{Q}_{TS}(u) \sim \frac{1+\left(\frac{r}{a}\right)^{d_w-d_f}u}{1+u}. \tag{110}$$

Note that the inverse Laplace transform of the above expression is naturally (40), along with (41). As opposed to the compact case, the timescale T_c now depends on the system size R. We

have plotted the evolution of the FPT probability distribution versus θ/Θ_c in Fig. 11, which confirms this result.

VI. CONCLUSION

We have presented in this paper the derivation of the FPT distribution to a target site for a random walker evolving in a bounded domain. We have shown that in the limit of large volume of the confining domain, this distribution falls into universality classes indexed by the walk dimension d_w and the fractal dimension d_f. We have extensively discussed the regime of validity of our results and shown that despite their asymptotic nature, they are robust and apply even for small system sizes and for a wide range of timescales.

This analysis puts forward the importance of the geometry, and in particular the position of the starting point, in the case of compact exploration. In the context of chemical reactions, this effect has been shown in Ref. [18] to lead to the so-called geometry-controlled kinetics. We stress that the decisive criterion for a reaction to be geometry controlled is the compact or noncompact nature of the transport and not its normal versus anomalous character.

These analytical results are validated by Monte Carlo simulations and exact enumeration methods, applied to various models, which illustrate the universality classes defined above. These schematic models have been widely used to describe transport in disordered media [19,20], for example, in the case of exciton trapping on percolation systems [21] or anomalous diffusion in biological cells [25–29], as a first step to account for geometrical obstruction and binding effects involved in real crowded environments. In particular, emblematic models of disordered systems have been studied in detail, such as random-trap and random-barrier models, models of diffusion on percolation clusters, and continuous-time random walks. Our approach also enables us to combine such models and consider, for example, continuous-time random walks on percolation clusters, which captures both geometric obstruction effects and binding effects and therefore might be relevant to model complex media such as cellular media.

APPENDIX A: SYMMETRY RELATIONS FOR W_{ji} AND H_{ji}

In this section, we derive some symmetry relations satisfied by both the propagator of the walk and the pseudo-Green function, under the detailed balance hypothesis (5). Iterating equation (1) over time yields

$$W_{ji}(n) = \sum_{k_{n-1}=1}^{N} \cdots \sum_{k_2=1}^{N} \sum_{k_1=1}^{N} w_{jk_{n-1}} \cdots w_{k_2k_1}\, w_{k_1i}. \quad \text{(A1)}$$

Let us multiply the above equation by W_i^{stat}, then, from (5), replace in the right member $w_{k_1i}\, W_i^{\text{stat}}$ by $W_{k_1}^{\text{stat}}\, w_{ik_1}$:

$$W_{ji}(n)\, W_i^{\text{stat}} = \sum_{k_{n-1}=1}^{N} \cdots \sum_{k_2=1}^{N} \sum_{k_1=1}^{N} w_{jk_{n-1}} \cdots w_{k_2k_1}\, W_{k_1}^{\text{stat}}\, w_{ik_1}. \quad \text{(A2)}$$

We repeat the replacement procedure through the whole hierarchy in (A2), and we eventually get

$$W_{ji}(n)\, W_i^{\text{stat}} = \sum_{k_{n-1}=1}^{N} \cdots \sum_{k_1=1}^{N} W_j^{\text{stat}}\, w_{k_{n-1}j} \cdots w_{k_1k_2}\, w_{ik_1}, \quad \text{(A3)}$$

where one recognizes, from (A1),

$$\sum_{k_{n-1}=1}^{N} \cdots \sum_{k_2=1}^{N} \sum_{k_1=1}^{N} w_{k_{n-1}j} \cdots w_{k_1k_2}\, w_{ik_1} = W_{ij}(n). \quad \text{(A4)}$$

We thus have

$$W_{ji}(n)\, W_i^{\text{stat}} = W_{ij}(n)\, W_j^{\text{stat}}, \quad \text{(A5)}$$

which constitutes a symmetry relation satisfied by the propagator. Using definition (6) for the pseudo-Green function, we also obtain

$$H_{ji}\, W_i^{\text{stat}} = H_{ij}\, W_j^{\text{stat}}. \quad \text{(A6)}$$

APPENDIX B: EXACT RECURRENCE EQUATION FOR THE FPT MOMENTS

Let us start by Laplace transforming Eq. (11):

$$\sum_{l=1}^{\infty} P_{TS}(l)\, e^{-(l-1)s} = \sum_{l=1}^{\infty} \sum_{j=1}^{N} w_{jS}\, P_{Tj}(l-1)\, e^{-(l-1)s}. \quad \text{(B1)}$$

Expanding the above equation in the neighborhood of $s = 0$ yields

$$\sum_{n=0}^{\infty} \frac{(-1)^n}{n!}\, s^n \sum_{k=0}^{n} \binom{n}{k} (-1)^k \left\langle \mathbf{T}_{TS}^{n-k} \right\rangle = \sum_{n=0}^{\infty} \frac{(-1)^n}{n!}\, s^n \sum_{j=1}^{N} w_{jS} \left\langle \mathbf{T}_{Tj}^{n} \right\rangle, \quad \text{(B2)}$$

from which we directly deduce the following hierarchy of equations for the FPT moments:

$$-\sum_{j=1}^{N} w_{jS} \left(\left\langle \mathbf{T}_{Tj}^{n} \right\rangle - \left\langle \mathbf{T}_{TS}^{n} \right\rangle \right) = \sum_{k=1}^{n} \binom{n}{k} (-1)^{k+1} \left\langle \mathbf{T}_{TS}^{n-k} \right\rangle, \quad \text{(B3)}$$

using Eq. (3). Let us rewrite (B3) as follows:

$$-\sum_{j=1}^{N} w_{jS}\, [f(j) - f(S)] = h(S), \quad \text{(B4)}$$

with $f(j) = \langle \mathbf{T}_{Tj}^{n} \rangle$, $f(j = T) = 0$, $f(S) = \langle \mathbf{T}_{TS}^{n} \rangle$, and $h(S) = \sum_{k=1}^{n} \binom{n}{k} (-1)^{k+1} \langle \mathbf{T}_{TS}^{n-k} \rangle$ respectively.

Actually, the Green function of Eq. (B4) reads

$$g_{lS} = \frac{W_l^{\text{stat}}}{W_T^{\text{stat}}} (H_{TT} - H_{TS}) + H_{lS} - H_{lT}. \quad \text{(B5)}$$

Indeed, we will now show that the recurrence relation

$$f(S) = \sum_{l=1}^{N} h(l) \left[\frac{W_l^{\text{stat}}}{W_T^{\text{stat}}} (H_{TT} - H_{TS}) + H_{lS} - H_{lT} \right] \quad \text{(B6)}$$

is the solution of (B4) along with the boundary condition $f(j=T)=0$.

Let us compute $\sum_{j=1}^{N} w_{jS}\,[f(j)-f(S)]$ by using expression (B6) for $f(j)$ and $f(S)$:

$$\sum_{j=1}^{N} w_{jS}\,[f(j)-f(S)] = \sum_{l=1}^{N} h(l)\left(W_l^{\rm stat}\frac{H_{TS}}{W_T^{\rm stat}}\sum_{j=1}^{N} w_{jS} - \frac{W_l^{\rm stat}}{W_T^{\rm stat}}\sum_{j=1}^{N} w_{jS}H_{Tj} + \sum_{j=1}^{N} w_{jS}H_{lj} - H_{lS}\sum_{j=1}^{N} w_{jS}\right). \tag{B7}$$

Using Eqs. (5), (7), and (10) of the main text, Eq. (B7) simplifies to

$$\sum_{j=1}^{N} w_{jS}\,[f(j)-f(S)] = -\sum_{l=1}^{N} h(l)\,\frac{W_l^{\rm stat}}{W_S^{\rm stat}}\,\delta_{l,S} = -h(S). \tag{B8}$$

The latter equality proves that expression (B6) is solution of the hierarchy of Eq. (B4). This finally yields Eq. (17), which we rewrite here explicitly:

$$\langle \mathbf{T}_{TS}^{n}\rangle = \frac{1}{W_T^{\rm stat}}\sum_{j=1}^{N}\sum_{k=1}^{n}\binom{n}{k}(-1)^{k+1} + \left[(H_{TT}-H_{TS})W_j^{\rm stat}(H_{jS}-H_{jT})W_T^{\rm stat}\right]\langle \mathbf{T}_{Tj}^{n-k}\rangle. \tag{B9}$$

APPENDIX C: EXPRESSIONS OF THE THIRD TO FIFTH FPT MOMENT COEFFICIENTS c_n IN THE COMPACT CASE

$$c_3 = 1+\frac{W_T^{\rm stat}}{H_{TT}^2}\sum_{k=1}^{N} H_{Tk}H_{kT} = \frac{(5d_w-2d_f)(d_f+d_w)^2}{4d_f\left(4d_w^2-d_f^2\right)}, \tag{C1}$$

$$\begin{aligned} c_4 &= 1+2\,\frac{W_T^{\rm stat}}{H_{TT}^2}\sum_{l=1}^{N} H_{Tl}\,H_{lT} + \frac{\left(W_T^{\rm stat}\right)^2}{H_{TT}^3}\sum_{j=1}^{N}\sum_{l=1}^{N} H_{Tj}\,H_{jl}\,H_{lT} \\ &= \frac{d_f^6-12d_f^4d_w^2+60d_f^2d_w^4+23d_w^6}{3\left(d_f^6-13d_f^4d_w^2+36d_f^2d_w^4\right)}, \end{aligned} \tag{C2}$$

$$\begin{aligned} c_5 &= 1+3\,\frac{W_T^{\rm stat}}{H_{TT}^2}\sum_{l=1}^{N} H_{Tl}H_{lT} + 2\,\frac{\left(W_T^{\rm stat}\right)^2}{H_{TT}^3}\sum_{k=1}^{N}\sum_{l=1}^{N} H_{Tk}H_{kl}H_{lT} \\ &\quad + \frac{\left(W_T^{\rm stat}\right)^2}{H_{TT}^4}\left(\sum_{l=1}^{N} H_{Tl}H_{lT}\right)^2 \\ &\quad + \frac{\left(W_T^{\rm stat}\right)^3}{H_{TT}^4}\sum_{j=1}^{N}\sum_{k=1}^{N}\sum_{l=1}^{N} H_{Tj}H_{jk}H_{kl}H_{lT} \\ &= \frac{5}{2d_f^3\left(d_f^2-4d_w^2\right)^2\left(d_f^4-25d_f^2d_w^2+144d_w^4\right)} \\ &\quad \times\left(8d_f^{11}-12d_f^{10}d_w-286d_f^9d_w^2+243d_f^8d_w^3+2906d_f^7d_w^4\right. \\ &\quad -3933d_f^6d_w^5-5642d_f^5d_w^6-5595d_f^4d_w^7-3674d_f^3d_w^8 \\ &\quad \left.+88605d_f^2d_w^9-45152d_fd_w^{10}+24372d_w^{11}\right). \end{aligned} \tag{C3}$$

APPENDIX D: O'SHAUGHNESSY-PROCACCIA TRANSPORT EQUATION

The O'Shaughnessy-Procaccia transport equation [38] describes the diffusion of a random walker evolving in a hyperspherically symmetric fractal domain of radius R and fractal dimension d_f. The dynamics of the random walker is characterized by the walk dimension d_w. The target is located at the center of the hypersphere. The size N of the domain reads

$$N = \Omega\, R^{d_f}, \tag{D1}$$

where Ω is the solid angle. The stationary propagator is given by

$$W_{\rm stat} = \frac{1}{N}, \tag{D2}$$

in agreement with hypothesis (4).

We consider a set of (hyper)spherical coordinates on the embedding space $\mathcal{E}$, where the radial coordinate is denoted by l. We have $\mathbf{r}_T = 0$. The volume of the region enclosed between a shell of radius l and a shell of radius $l+dl$ is

$$d\mu = \Omega\, d_f\, l^{d_f-1}\, dl. \tag{D3}$$

1. Compact exploration

Propagator and pseudo-Green function. Let $r=|\mathbf{r}_T-\mathbf{r}_S|$. We denote by $W(r,t|0)$ the propagor of the walk, defined with respect to the volume element $d\mu$ given by (D3). The O'Shaughessy-Procaccia transport equation reads [38]

$$\partial_t W(r,t|0) = \mathcal{L}\,W(r,t|0) + \delta(t)\delta(r), \tag{D4}$$

where the operator $\mathcal{L}$ is given by

$$\mathcal{L}\,W(r,t|0) = \frac{K}{r^{d_f-1}}\partial_r[r^{d_f-d_w+1}\partial_r W(r,t|0)], \tag{D5}$$

and K is the generalized diffusion coefficient. The propagator $W(r,t|0)$ satisfies the boundary condition

$$\partial_r W(r,t|0)_{|r=R} = 0, \tag{D6}$$

and the normalization condition

$$\Omega\, d_f\int_0^R W(r,t|0)\, r^{d_f-1}\, dr = 1 \quad \forall\, t. \tag{D7}$$

We solve Eq. (D4) in Laplace space, and we get, for the Laplace transform $\hat{W}(r,s|0)$ of $W(r,t|0)$:

$$\hat{W}(r,s|0) = \frac{\Gamma(-\nu)}{\Omega K d_w^{\nu+1}} r^{\frac{d_w-d_f}{2}} \left(\frac{s}{K}\right)^{\frac{\nu-1}{2}} \frac{I_{1-\nu}\left(\frac{2r^{d_w/2}\sqrt{\frac{s}{K}}}{d_w}\right) I_\nu\left(\frac{2R^{d_w/2}\sqrt{\frac{s}{K}}}{d_w}\right) - I_{\nu-1}\left(\frac{2r^{d_w/2}\sqrt{\frac{s}{K}}}{d_w}\right) I_{-\nu}\left(\frac{2R^{d_w/2}\sqrt{\frac{s}{K}}}{d_w}\right)}{I_\nu\left(\frac{2R^{d_w/2}\sqrt{\frac{s}{K}}}{d_w}\right)}, \tag{D8}$$

where $\nu = d_f/d_w$. The pseudo-Green function is given by

$$H_{TS} = \tilde{G}(r|0) = \int_0^\infty \left(W(r,t|0) - \frac{1}{N}\right) dt \tag{D9}$$

and satisfies the transport equation

$$\mathcal{L}\,\tilde{G}(r|0) = \frac{1}{N} - \delta(r), \tag{D10}$$

with the boundary condition $\tilde{G}'(R|0) = 0$ and the condition

$$\Omega\, d_f \int_0^R \tilde{G}(r|0)\, r^{d_f-1} dr = 0. \tag{D11}$$

We get

$$H_{TS} = \tilde{G}(r|0) = \frac{r^{d_w}}{K\Omega R^{d_f} d_f d_w} - \frac{r^{d_w-d_f}}{K\Omega d_f (d_w-d_f)} + \frac{2d_f R^{d_w-d_f}}{K\Omega d_w\left(d_w^2-d_f^2\right)}. \tag{D12}$$

In particular,

$$H_{TT} = \tilde{G}(0|0) = \frac{2d_f R^{d_w-d_f}}{K\Omega d_w\left(d_w^2-d_f^2\right)}. \tag{D13}$$

In the large-volume limit ($R \gg r$), we have

$$H_{TS} = \frac{2d_f R^{d_w-d_f}}{K\Omega d_w\left(d_w^2-d_f^2\right)}, \tag{D14}$$

$$\langle \mathbf{T}_{TS}\rangle = \frac{H_{TT}-H_{TS}}{W^{\rm stat}} = \frac{R^{d_f}\, r^{d_w-d_f}}{K d_f (d_w-d_f)}, \tag{D15}$$

and

$$\overline{\langle \mathbf{T}\rangle}_T = \frac{H_{TT}}{W^{\rm stat}} = \frac{2d_f R^{d_w}}{K d_w\left(d_w^2-d_f^2\right)}. \tag{D16}$$

Thus,

$$\frac{\langle \mathbf{T}_{TS}\rangle}{\overline{\langle \mathbf{T}\rangle}_T} = \frac{H_{TT}-H_{TS}}{H_{TT}} = \frac{d_w(d_w+d_f)}{2d_f^2}\left(\frac{r}{R}\right)^{d_w-d_f}. \tag{D17}$$

Now that we have an expression for the Laplace transform $\hat{W}(r,s|0)$ of the propagator [see Eq. (D8)], it is possible to compute the sums $\mathcal{S}_{TT,n}$ and $\tilde{\mathcal{S}}_{TS,n}$, defined by (E19) and (E20), respectively (see Appendix G for the computation method). We get

$$\mathcal{S}_{TT,1} = \frac{d_f(2d_f+5d_w)R^{2d_w-d_f}}{d_w^2(d_f+d_w)^2\left(4d_w^2-d_f^2\right)K^2\Omega}, \quad \tilde{\mathcal{S}}_{TS,1} = \frac{2r^{d_w}R^{d_w-d_f}}{d_w^2(d_w-d_f)(d_f+d_w)K^2\Omega}, \tag{D18}$$

$$\mathcal{S}_{TT,2} = \frac{4d_f\left(2d_f^2+13d_wd_f+23d_w^2\right)R^{3d_w-d_f}}{3d_w^3(d_f+d_w)^3(d_f+2d_w)\left(9d_w^2-d_f^2\right)K^3\Omega}, \quad \tilde{\mathcal{S}}_{TS,2} = \frac{2\,(2d_f+5d_w)r^{d_w}R^{2d_w-d_f}}{d_w^3(d_f+d_w)^2\left(4d_w^2-d_f^2\right)K^3\Omega}, \tag{D19}$$

$$\mathcal{S}_{TT,3} = \frac{d_f\left(4d_f^4+56d_wd_f^3+303d_w^2d_f^2+748d_w^3d_f+677d_w^4\right)R^{4d_w-d_f}}{d_w^4(d_f+d_w)^4(d_f+2d_w)^2(d_f+3d_w)\left(16d_w^2-d_f^2\right)K^4\Omega},$$
$$\tilde{\mathcal{S}}_{TS,3} = \frac{2\left(2d_f^2+13d_wd_f+23d_w^2\right)r^{d_w}R^{3d_w-d_f}}{3d_w^4(d_f+d_w)^3\left(-d_f^3-2d_wd_f^2+9d_w^2d_f+18d_w^3\right)K^4\Omega}, \tag{D20}$$

$$\mathcal{S}_{TT,4} = \frac{8d_f\left(4d_f^5+84d_wd_f^4+731d_w^2d_f^3+3319d_w^3d_f^2+7821d_w^4d_f+7313d_w^5\right)R^{5d_w-d_f}}{5d_w^5(d_f+d_w)^5(d_f+2d_w)^2(d_f+3d_w)(d_f+4d_w)\left(25d_w^2-d_f^2\right)K^5\Omega},$$
$$\tilde{\mathcal{S}}_{TS,4} = \frac{4\left(4d_f^4+56d_wd_f^3+303d_w^2d_f^2+748d_w^3d_f+677d_w^4\right)r^{d_w}R^{4d_w-d_f}}{d_w^5(d_f+d_w)^4(d_f+2d_w)^2\left(-d_f^3-3d_wd_f^2+16d_w^2d_f+48d_w^3\right)K^5\Omega}. \tag{D21}$$

FPT distribution probability. The FPT probability density $P(r,t|0)$ satisfies

$$\partial_t P(r,t|0) = \mathcal{L}P(r,t|0), \tag{D22}$$

where $\mathcal{L}$ is given by (D5). The function P obeys the following boundary conditions:

$$P(0,t|0) = \delta(t), \quad \partial_r P(r,t|0)_{|r=R} = 0. \tag{D23}$$

By solving the Laplace-transformed equations above, we get

$$\hat{P}(r,s|0) = d_w^{\nu-1} r^{\frac{d_w-d_f}{2}} \left(\frac{s}{K}\right)^{\frac{1-\nu}{2}} \frac{\Gamma(\nu)}{I_{-\nu}[x(R,s)]} \times \{I_{\nu-1}[x(r,s)]I_{-\nu}[x(R,s)] - I_{1-\nu}[x(r,s)]I_{\nu}[x(R,s)]\}, \quad \text{(D24)}$$

where

$$x(r,s) = \frac{2}{d_w\sqrt{K}}\sqrt{r^{d_w}s}. \quad \text{(D25)}$$

2. Noncompact exploration

Propagator and pseudo-Green function. Let a be a characteristic length scale, of the order of one step length. The propagator $W(r,t|a)$ verifies

$$\partial_t W(r,t|a) = \mathcal{L}W(r,t|a) + \delta(t)\delta(r-a), \quad \text{(D26)}$$

where $\mathcal{L}$ is given by (D5). The propagator $W(r,t|a)$ satisfies the boundary condition

$$\partial_r W(r,t|a)_{|r=R} = 0, \quad \text{(D27)}$$

and the normalization condition, at all times:

$$d_f \Omega \int_a^R W(r,t|a) r^{d_f-1} dr = 1. \quad \text{(D28)}$$

We solve Eq. (D26) in Laplace space, for the Laplace transform $\hat{W}(r,s|a)$, and we get

$$\hat{W}(r,s|a) = \frac{a^{-\frac{d_f}{2}} r^{\frac{d_w}{2}-\frac{d_f}{2}}}{d_f\sqrt{Ks}\,\Omega} \frac{I_{\nu-1}[x(r,s)]\,I_{-\nu}[x(R,s)] - I_{1-\nu}[x(r,s)]\,I_{\nu}[x(R,s)]}{I_{-\nu}[x(a,s)]\,I_{\nu}[x(R,s)] - I_{-\nu}[x(R,s)]\,I_{\nu}[x(a,s)]}. \quad \text{(D29)}$$

For $r = a$:

$$\hat{W}(a,s|a) = \frac{a^{\frac{1}{2}(d_w-2d_f)}}{d_f\sqrt{Ks}\,\Omega} \frac{I_{1-\nu}[x(a,s)]\,I_{\nu}[x(R,s)] - I_{\nu-1}[x(,s)]\,I_{-\nu}[x(R,s)]}{I_{-\nu}[x(R,s)]\,I_{\nu}[x(a,s)] - I_{-\nu}[x(a,s)]\,I_{\nu}[x(R,s)]}. \quad \text{(D30)}$$

The pseudo-Green function $H_{TS} = \tilde{G}(r|a)$ satisfies

$$\mathcal{L}\tilde{G}(r|a) = \frac{1}{\Omega(R^{d_f}-a^{d_f})} - \delta(r-a), \quad \text{(D31)}$$

where $\mathcal{L}$ is given by (D5). The function $\tilde{G}$ satisfies the boundary condition, $\tilde{G}'(R|a) = 0$, and the condition

$$d_f\,\Omega \int_a^R \tilde{G}(r|a) r^{d_f-1} = 0. \quad \text{(D32)}$$

We thus get

$$H_{TS} = \tilde{G}(r|a) = \frac{r^{d_w}}{K\Omega d_f d_w (R^{d_f}-a^{d_f})} - \frac{R^{d_f} r^{d_w-d_f}}{K\Omega d_f (d_w-d_f)(R^{d_f}-a^{d_f})} + b, \quad \text{(D33)}$$

where

$$b = \frac{R^{d_f}(R^{d_w}-a^{d_w})}{K\,\Omega\,d_w\,(d_w-d_f)(R^{d_f}-a^{d_f})^2} - \frac{R^{d_w+d_f}-a^{d_w+d_f}}{K\,\Omega\,d_w\,(d_w+d_f)(R^{d_f}-a^{d_f})^2}, \quad \text{(D34)}$$

and

$$H_{TT} = \tilde{G}(a|a) = \frac{a^{d_w}}{K\Omega d_f d_w (R^{d_f}-a^{d_f})} - \frac{R^{d_f} a^{d_w-d_f}}{K\Omega d_f (d_w-d_f)(R^{d_f}-a^{d_f})} + b. \quad \text{(D35)}$$

In the large-volume limit, one has

$$H_{TS} = \frac{R^{d_f} r^{d_w-d_f}}{K\Omega d_f (d_f-d_w)(R^{d_f}-a^{d_f})}, \quad \text{(D36)}$$

$$H_{TT} = \frac{R^{d_f} a^{d_w-d_f}}{K\Omega d_f (d_f-d_w)(R^{d_f}-a^{d_f})}, \quad \text{(D37)}$$

$$\langle \mathbf{T}_{TS} \rangle = \frac{H_{TT}-H_{TS}}{W^{\text{stat}}} = \frac{R^{d_f} a^{d_w-d_f}}{K\Omega d_f (d_f-d_w)(R^{d_f}-a^{d_f})}\left[1-\left(\frac{r}{a}\right)^{d_w-d_f}\right], \quad \text{(D38)}$$

$$\overline{\langle \mathbf{T} \rangle}_T = \frac{H_{TT}}{W^{\text{stat}}} = \frac{R^{d_f} a^{d_w-d_f}}{K\Omega d_f (d_f-d_w)(R^{d_f}-a^{d_f})}, \quad \text{(D39)}$$

and

$$\frac{\langle \mathbf{T}_{TS} \rangle}{\overline{\langle \mathbf{T} \rangle}_T} = \frac{H_{TT}-H_{TS}}{H_{TT}} = \left(1-\left(\frac{r}{a}\right)^{d_w-d_f}\right). \quad \text{(D40)}$$

FPT distribution probability. The probability density $P(r,t|a)$ obeys the following equation, for $r > a$:

$$\partial_t P(r,t|a) = \mathcal{L}P(r,t|a), \quad \text{(D41)}$$

where $\mathcal{L}$ is given by (D5), along with the boundary conditions:

$$P(a,t|a) = \delta(t), \quad \partial_r P(r,t|a)_{|r=R} = 0. \quad \text{(D42)}$$

Solving the above equation in Laplace space, we get

$$\hat{P}(r,s|a) = \left(\frac{a}{r}\right)^{\frac{d_f-d_w}{2}} \frac{I_{\nu-1}[x(r,s)]I_{-\nu}[x(R,s)] - I_{1-\nu}[x(r,s)]I_{\nu}[x(R,s)]}{I_{\nu-1}[x(a,s)]I_{-\nu}[x(R,s)] - I_{1-\nu}[x(a,s)]I_{\nu}[x(R,s)]}, \tag{D43}$$

where x is defined by (D25).

APPENDIX E: DERIVATION OF THE FPT MOMENTS

1. Noncompact case

Expression of the nth FPT moment. We will prove by recurrence that, under the assumption

$$\sum_{j=1}^{N} H_{Tj}\,(H_{jT} - H_{jS}) = \mathcal{O}\big[\big(W_T^{\rm stat}\big)^{-1-\frac{2}{d_f}(d_w-d_f)}\big], \tag{E1}$$

the nth FPT moment reads, in the large-volume limit:

$$\big\langle \mathbf{T}_{TS}^{n}\big\rangle \sim \frac{n!}{\big(W_T^{\rm stat}\big)^{n}}\, H_{TT}^{n-1}\,(H_{TT} - H_{TS}) + \mathcal{O}\big[\big(W_T^{\rm stat}\big)^{-n-\frac{2}{d_f}(d_w-d_f)}\big]. \tag{E2}$$

One can easily check that (E2) is true for $n = 1$ [see expression (18) of the first FPT moment]. Let us now demonstrate that if (E2) is true at the nth order, then it is also true at the $(n+1)$th order. To do so, we first recall that in the noncompact case, the pseudo-Green function is finite in the large-volume limit [see comment before Eq. (22)]. Let us use the recurrence relation (21). Replacing $\langle \mathbf{T}_{Tj}^{n}\rangle$ by expression (E2) into (21) yields

$$\big\langle \mathbf{T}_{TS}^{n+1}\big\rangle = \frac{(n+1)!}{\big(W_T^{\rm stat}\big)^{n+1}}\, H_{TT}^{n-1} \sum_{j=1}^{N}\big[(H_{TT} - H_{TS})\, W_j^{\rm stat} + \big(H_{jS} - H_{jT}\big)\, W_T^{\rm stat}\big]\big\{\big(H_{TT} - H_{Tj}\big) + \mathcal{O}\big[\big(W_T^{\rm stat}\big)^{-\frac{2}{d_f}(d_w-d_f)}\big]\big\}, \tag{E3}$$

where we used the fact that $H_{TT} = \mathcal{O}(1)$. Using Eqs. (2), (10), and (8), we simplify (E3) into

$$\big\langle \mathbf{T}_{TS}^{n+1}\big\rangle = \frac{(n+1)!}{\big(W_T^{\rm stat}\big)^{n+1}}\, H_{TT}^{n-1}\Bigg\{H_{TT}\,(H_{TT} - H_{TS}) + W_T^{\rm stat}\sum_{j=1}^{N} H_{Tj}(H_{jT} - H_{jS}) + \mathcal{O}\big[\big(W_T^{\rm stat}\big)^{-\frac{2}{d_f}(d_w-d_f)}\big]\Bigg\}. \tag{E4}$$

Using assumption (E1), (E4) reduces to

$$\big\langle \mathbf{T}_{TS}^{n+1}\big\rangle = \frac{(n+1)!}{\big(W_T^{\rm stat}\big)^{n+1}}\, H_{TT}^{n}\,(H_{TT} - H_{TS}) + \mathcal{O}\big[\big(W_T^{\rm stat}\big)^{-n-1-\frac{2}{d_f}(d_w-d_f)}\big], \tag{E5}$$

which proves (E2). Note that expression (E2) ensures that Eq. (20) is satisfied.

Validity of the hypothesis. We now argue that assumption (E1) is satisfied in a wide range of situations. We consider the general example of a scale-invariant problem, in which the unbounded propagator satisfies the standard scaling [19]:

$$W_{ji}^{\infty}(n) \sim n^{-\frac{d_f}{d_w}}\, f\left(\frac{\rho_{ji}}{n^{1/d_w}}\right), \tag{E6}$$

where $\rho_{ji} = |\,\mathbf{r}_j - \mathbf{r}_i\,|$. and the stationary probability is uniform:

$$W_j^{\rm stat} = \frac{1}{N} \quad \forall\ j. \tag{E7}$$

Note that the condition (4) is fulfilled. The pseudo-Green function thus verifies in the large-volume limit

$$H_{ji} \sim C\,\rho_{ji}^{d_w-d_f}, \tag{E8}$$

where C is a constant.

Let us evaluate the order of magnitude of $\sum_{j=1}^{N} H_{Tj}\,(H_{jT} - H_{jS})$ in that case. Since the pseudo-Green function is symmetric in its indices when the stationary propagator is uniform [see (A6)]:

$$\sum_{j=1}^{N} H_{Tj}\,(H_{jT} - H_{jS}) = \sum_{j=1}^{N} H_{jT}^{2} - \sum_{j=1}^{N} H_{jT}\,H_{jS}. \tag{E9}$$

Let $\mathcal{E}$ be the d-dimensional Euclidean space ($d \geqslant d_f$) in which the confining domain $\mathcal{D}$ is embedded. We consider a set of (hyper)spherical coordinates on $\mathcal{E}$. We assume the considered system to be (hyper)spherically symmetric. The target is taken to be at the origin of the coordinate system: $\mathbf{r}_T = 0$. Let Ω be the solid angle, and let l be the radial coordinate. The volume element between a shell of radius l and a shell of radius $l + dl$ is $d\mu = \Omega\, d_f\, l^{d_f-1}\, dl$. We then have

$$\begin{aligned}\sum_{l=1}^{N} H_{jT}^{2} &= \int_{\mathcal{D}} H_{jT}^{2}\, d\mu \\ &= \Omega\, d_f \int_{0}^{N^{1/d_f}} H_{jT}^{2} r_j^{d_f-1}\, dr_j \\ &\sim \frac{C^2\,\Omega}{2\,d_w - d_f}\, N^{\frac{2d_w-d_f}{d_f}},\end{aligned} \tag{E10}$$

where $r_j = |\,\mathbf{r}_j\,|$, and where expression (E8) for H_{ji} was used. On the other hand, we have

$$\sum_{j=1}^{N} H_{jT}\,H_{jS} \leqslant \left(\sum_{j=1}^{N} H_{jT}^{2}\sum_{j=1}^{N} H_{jS}^{2}\right)^{\frac{1}{2}}, \tag{E11}$$

which implies that

$$\sum_{j=1}^{N} H_{jT}\,H_{jS} = \mathcal{O}\big(N^{\frac{2d_w-d_f}{d_f}}\big). \tag{E12}$$

Hence

$$\sum_{j=1}^{N} H_{Tj}\,(H_{jT} - H_{jS}) = \mathcal{O}\big(N^{\frac{2d_w - d_f}{d_f}}\big), \tag{E13}$$

which confirms hypothesis (E1).

2. Compact case

We get iteratively from (21) the following expressions for the first moments:

$$\frac{\langle \mathbf{T}_{TS}\rangle}{\overline{\langle \mathbf{T}\rangle}_T} = \frac{H_{TT} - H_{TS}}{H_{TT}}, \tag{E14}$$

$$\frac{\langle \mathbf{T}_{TS}^2\rangle}{\overline{\langle \mathbf{T}\rangle}_T^2} = 2\,\frac{H_{TT} - H_{TS}}{H_{TT}} + 2\,\frac{W_T^{\mathrm{stat}}}{H_{TT}^2}\sum_{l=1}^{N} H_{Tl}\,(H_{lT} - H_{lS}), \tag{E15}$$

$$\begin{aligned}\frac{\langle \mathbf{T}_{TS}^3\rangle}{\overline{\langle \mathbf{T}\rangle}_T^3} = {} & 6\,\frac{H_{TT} - H_{TS}}{H_{TT}}\left(1 + \frac{W_T^{\mathrm{stat}}}{H_{TT}^2}\sum_{l=1}^{N} H_{Tl}H_{lT}\right) + 6\,\frac{W_T^{\mathrm{stat}}}{H_{TT}^2}\sum_{l=1}^{N} H_{Tl}\,(H_{lT} - H_{lS}) \\ & + 6\,\frac{\big(W_T^{\mathrm{stat}}\big)^2}{H_{TT}^3}\sum_{j=1}^{N}\sum_{l=1}^{N} H_{Tj}H_{jl}\,(H_{lT} - H_{lS}),\end{aligned} \tag{E16}$$

$$\begin{aligned}\frac{\langle \mathbf{T}_{TS}^4\rangle}{\overline{\langle \mathbf{T}\rangle}_T^4} = {} & 24\,\frac{H_{TT} - H_{TS}}{H_{TT}}\left[1 + 2\,\frac{W_T^{\mathrm{stat}}}{H_{TT}^2}\sum_{l=1}^{N} H_{Tl}\,H_{lT} + \frac{\big(W_T^{\mathrm{stat}}\big)^2}{H_{TT}^3}\sum_{j=1}^{N}\sum_{l=1}^{N} H_{Tj}\,H_{jl}\,H_{lT}\right] \\ & + 24\,\frac{W_T^{\mathrm{stat}}}{H_{TT}^2}\left(1 + \frac{W_T^{\mathrm{stat}}}{H_{TT}^2}\sum_{l=1}^{N} H_{Tl}H_{lT}\right)\left[\sum_{l=1}^{N} H_{Tl}\,(H_{lT} - H_{lS})\right] + 24\,\frac{\big(W_T^{\mathrm{stat}}\big)^2}{H_{TT}^3}\sum_{j=1}^{N}\sum_{l=1}^{N} H_{Tj}H_{jl}\,(H_{lT} - H_{lS}) \\ & + 24\,\frac{\big(W_T^{\mathrm{stat}}\big)^3}{H_{TT}^4}\sum_{j=1}^{N}\sum_{k=1}^{N}\sum_{l=1}^{N} H_{Tj}\,H_{jk}\,H_{kl}\,(H_{lT} - H_{lS}),\end{aligned} \tag{E17}$$

and

$$\begin{aligned}\frac{\langle \mathbf{T}_{TS}^5\rangle}{\overline{\langle \mathbf{T}\rangle}_T^5} = {} & 120\,\frac{H_{TT} - H_{TS}}{H_{TT}}\left[1 + 3\,\frac{W_T^{\mathrm{stat}}}{H_{TT}^2}\sum_{l=1}^{N} H_{Tl}H_{lT} + 2\,\frac{\big(W_T^{\mathrm{stat}}\big)^2}{H_{TT}^3}\sum_{k=1}^{N}\sum_{l=1}^{N} H_{Tk}H_{kl}H_{lT} + \frac{\big(W_T^{\mathrm{stat}}\big)^2}{H_{TT}^4}\left(\sum_{l=1}^{N} H_{Tl}H_{lT}\right)^2\right. \\ & \left. + \frac{\big(W_T^{\mathrm{stat}}\big)^3}{H_{TT}^4}\sum_{j=1}^{N}\sum_{k=1}^{N}\sum_{l=1}^{N} H_{Tj}H_{jk}H_{kl}H_{lT}\right] \\ & + 120\,\frac{W_T^{\mathrm{stat}}}{H_{TT}^2}\left[1 + 2\,\frac{W_T^{\mathrm{stat}}}{H_{TT}^2}\sum_{l=1}^{N} H_{Tl}H_{lT} + \frac{\big(W_T^{\mathrm{stat}}\big)^2}{H_{TT}^3}\sum_{k=1}^{N}\sum_{l=1}^{N} H_{Tk}H_{kl}H_{lT}\right]\sum_{l=1}^{N} H_{Tl}(H_{lT} - H_{lS}) \\ & + 120\,\frac{\big(W_T^{\mathrm{stat}}\big)^2}{H_{TT}^3}\left(1 + \frac{W_T^{\mathrm{stat}}}{H_{TT}^2}\sum_{l=1}^{N} H_{Tl}H_{lT}\right)\sum_{k=1}^{N}\sum_{l=1}^{N} H_{Tk}H_{kl}(H_{lT} - H_{lS}) \\ & + 120\,\frac{\big(W_T^{\mathrm{stat}}\big)^3}{H_{TT}^4}\sum_{j=1}^{N}\sum_{k=1}^{N}\sum_{l=1}^{N} H_{Tj}H_{jk}H_{kl}(H_{lT} - H_{lS}) + 120\,\frac{\big(W_T^{\mathrm{stat}}\big)^4}{H_{TT}^5}\sum_{i=1}^{N}\sum_{j=1}^{N}\sum_{k=1}^{N}\sum_{l=1}^{N} H_{Ti}H_{ij}H_{jk}H_{kl}(H_{lT} - H_{lS}).\end{aligned} \tag{E18}$$

It is shown in Appendix G that sums of the form

$$\mathcal{S}_{TT,n} = \sum_{k_1=1}^{N} \cdots \sum_{k_{n-1}=1}^{N} \sum_{k_n=1}^{N} H_{Tk_1} \cdots H_{k_{n-1}k_n} H_{k_nT} \quad \text{(E19)}$$

and of the form

$$\begin{aligned}\tilde{\mathcal{S}}_{TS,n} &= \sum_{k_1=1}^{N} \cdots \sum_{k_{n-1}=1}^{N} \sum_{k_n=1}^{N} H_{Tk_1} \cdots H_{k_{n-1}k_n} \left(H_{k_nT} - H_{k_nS}\right) \\ &= \mathcal{S}_{TT,n} - \mathcal{S}_{TS,n} \end{aligned} \quad \text{(E20)}$$

can be rewritten in a simpler, more tractable way, in terms of the Laplace transform of the propagator.

We now evaluate the orders of magnitude of the terms involved in the above expressions of the FPT moments. In case of compact exploration, the mean number of visits of site j for a random walker starting from site i is infinite (in absence of confinement). In other words, the sum $\sum_{n=0}^{\infty} W_{ji}^{\infty}(n)$ now diverges, and the Green function G_{ji}, which constitutes the leading-order term of the pseudo-Green function in the large-volume limit, is therefore no longer defined. In the case when one has to deal with differences of Green functions, this divergence may be avoided [17]. But here we have to compute terms involving pseudo-Green functions alone and products of pseudo-Green functions. It is therefore now necessary to go further and to know how H depends on the volume N.

The derivation of the expressions of the FPT moments in the large-volume limit is presented here in detail for the instructive case of the third FPT moment. With the help of the quantities computed with the O'Shaughnessy-Procaccia transport equation, we evaluate the orders of magnitude of the various terms involved in expression (E16) of $\langle \mathbf{T}_{TS}^3 \rangle / \overline{\langle \mathbf{T} \rangle}_T^3$. Using expressions (D2), (D13), (D14), and (D18) for W_T^{stat}, H_{TT}, $H_{TT} - H_{TS}$, and $\mathcal{S}_{TT,1}$, respectively, we get

$$6\,\frac{H_{TT} - H_{TS}}{H_{TT}} \left(1 + \frac{W_T^{\text{stat}}}{H_{TT}^2} \sum_{l=1}^{N} H_{Tl} H_{lT}\right) = 3\,\frac{d_w(d_w + d_f)}{d_f^2} \left(\frac{r}{R}\right)^{d_w - d_f} \left[1 + \frac{(d_w - d_f)^2 (2d_f + 5d_w)}{4\,d_f \left(4d_w^2 - d_f^2\right)}\right]. \quad \text{(E21)}$$

Similarly

$$6\,\frac{W_T^{\text{stat}}}{H_{TT}^2} \sum_{l=1}^{N} H_{Tl}\,(H_{lT} - H_{lS}) = 3\frac{d_w^2 - d_f^2}{d_f^2} \left(\frac{r}{R}\right)^{d_w} \quad \text{(E22)}$$

and

$$6\,\frac{\left(W_T^{\text{stat}}\right)^2}{H_{TT}^3} \sum_{j=1}^{N} \sum_{l=1}^{N} H_{Tj} H_{jl}\,(H_{lT} - H_{lS}) = \frac{3(d_f - d_w)^3 (d_f + d_w)(2d_f + 5d_w)}{2d_f^3 \left(d_f^2 - 4d_w^2\right)} \left(\frac{r}{R}\right)^{d_w}. \quad \text{(E23)}$$

In the large-volume limit, i.e., for $\frac{r}{R} \ll 1$, the third FPT moment therefore reads

$$\frac{\langle \mathbf{T}_{TS}^3 \rangle}{\overline{\langle \mathbf{T} \rangle}_T^3} = 6 \left(1 + \frac{W_T^{\text{stat}}}{H_{TT}^2} \sum_{l=1}^{N} H_{Tl} H_{lT}\right) \frac{H_{TT} - H_{TS}}{H_{TT}} = \frac{3(5d_w - 2d_f)(d_f + d_w)^2}{2d_f \left(4d_w^2 - d_f^2\right)} \frac{H_{TT} - H_{TS}}{H_{TT}}. \quad \text{(E24)}$$

In the same way, we obtain

$$\frac{\langle \mathbf{T}_{TS} \rangle}{\overline{\langle \mathbf{T} \rangle}_T} = \frac{H_{TT} - H_{TS}}{H_{TT}}, \quad \text{(E25)}$$

$$\frac{\langle \mathbf{T}_{TS}^2 \rangle}{\overline{\langle \mathbf{T} \rangle}_T^2} = 2\,\frac{H_{TT} - H_{TS}}{H_{TT}}, \quad \text{(E26)}$$

$$\begin{aligned}\frac{\langle \mathbf{T}_{TS}^4 \rangle}{\overline{\langle \mathbf{T} \rangle}_T^4} &= 24 \left[1 + 2\,\frac{W_T^{\text{stat}}}{H_{TT}^2} \sum_{l=1}^{N} H_{Tl}\,H_{lT} + \frac{\left(W_T^{\text{stat}}\right)^2}{H_{TT}^3} \sum_{j=1}^{N} \sum_{l=1}^{N} H_{Tj}\,H_{jl}\,H_{lT}\right] \frac{H_{TT} - H_{TS}}{H_{TT}} \\ &= \frac{8\left(d_f^6 - 12 d_f^4 d_w^2 + 60 d_f^2 d_w^4 + 23 d_w^6\right)}{d_f^6 - 13 d_f^4 d_w^2 + 36 d_f^2 d_w^4} \frac{H_{TT} - H_{TS}}{H_{TT}}, \end{aligned} \quad \text{(E27)}$$

and

$$\begin{aligned}\frac{\langle \mathbf{T}_{TS}^5 \rangle}{\overline{\langle \mathbf{T} \rangle}_T^5} = 120 \Bigg[1 &+ 3\,\frac{W_T^{\text{stat}}}{H_{TT}^2} \sum_{l=1}^{N} H_{Tl} H_{lT} + 2\,\frac{\left(W_T^{\text{stat}}\right)^2}{H_{TT}^3} \sum_{k=1}^{N} \sum_{l=1}^{N} H_{Tk} H_{kl} H_{lT} + \frac{\left(W_T^{\text{stat}}\right)^2}{H_{TT}^4} \left(\sum_{l=1}^{N} H_{Tl} H_{lT}\right)^2 \\ &+ \frac{\left(W_T^{\text{stat}}\right)^3}{H_{TT}^4} \sum_{j=1}^{N} \sum_{k=1}^{N} \sum_{l=1}^{N} H_{Tj} H_{jk} H_{kl} H_{lT}\Bigg] \frac{H_{TT} - H_{TS}}{H_{TT}} \end{aligned}$$

$$= \frac{5}{2d_f^3\left(d_f^2-4d_w^2\right)^2\left(d_f^4-25d_f^2d_w^2+144d_w^4\right)}\left[8d_f^{11}-12d_f^{10}d_w-286d_f^9d_w^2+243d_f^8d_w^3+2906d_f^7d_w^4\right.$$
$$-3933d_f^6d_w^5-5642d_f^5d_w^6-5595d_f^4d_w^7-3674d_f^3d_w^8+88605d_f^2d_w^9$$
$$\left.-45152d_fd_w^{10}+24372d_w^{11}\right]\frac{H_{TT}-H_{TS}}{H_{TT}}. \quad \text{(E28)}$$

APPENDIX F: COMPUTATION OF THE FPT DISTRIBUTION IN THE CASE OF COMPACT EXPLORATION

In this Section, we compute the inverse-Laplace transform of the function $\hat{\chi}^\sigma$ involved in Eqs. (35) and (33), which we rewrite as

$$\hat{\chi}^\sigma(s) = As^{1-\nu}\frac{I_\nu[X(s)]}{I_{-\nu}[X(s)]}e^{-s/\sigma}, \quad \text{(F1)}$$

where we recall that $\nu = d_f/d_w$, and

$$A = \frac{2^{\nu-1}d_f^{\nu-1}d_w^{\nu-1}}{\left(d_w^2-d_f^2\right)^{\nu-1}}\frac{\Gamma(\nu)}{\Gamma(2-\nu)}\overline{\langle\mathbf{T}\rangle}_T^{1-\nu}, \quad \text{(F2)}$$

$$X(s) = Bs^{1/2}, \quad \text{(F3)}$$

$$\text{with} \quad B = \left[\frac{2\left(d_w^2-d_f^2\right)}{d_wd_f}\overline{\langle\mathbf{T}\rangle}_T\right]^{1/2}. \quad \text{(F4)}$$

According to Bromwich formula, the inverse-Laplace transform χ^σ of $\hat{\chi}^\sigma$ is given by

$$\chi^\sigma(t) = \frac{1}{2i\pi}\lim_{R\to\infty}\int_{\mathcal{C}_1}F(z)\exp\left[z(t-1/\sigma)\right], \quad \text{(F5)}$$

where $\mathcal{C}_1$ is drawn on Fig. 12, with the convention that R stands for the radius of the semicircular contour $\mathcal{C}$, and

$$F(z) = Az^{1-\nu}\frac{I_\nu[Y(z)]}{I_{-\nu}[Y(z)]}, \quad \text{(F6)}$$

$$Y(z) = Bz^{1/2}. \quad \text{(F7)}$$

To define the functions $(\bullet)^{1/2}$ and $(\bullet)^{1-\nu}$, we take the cut in the complex plane to be the negative real axis, including the origin. Let $z = \rho\exp(i\theta)$, we take the determinations $z^{1/2} = \rho^{1/2}\exp(i\theta/2)$ and $z^{1-\nu} = \rho^{1-\nu}\exp(i(1-\nu)\theta)$. For latter purpose, we rewrite the function F in the equivalent form:

$$F(z) = Az^{1-\nu}i^{-2\nu}\frac{J_\nu[iY(z)]}{J_{-\nu}[iY(z)]}. \quad \text{(F8)}$$

One verifies easily that F has an infinite number of poles, given by $z_k = -\alpha_k^2/B^2$ for $k \geqslant 1$, where the α_k denote the strictly positive zeros of the Bessel function $J_{-\nu}$: $0 < \alpha_1 < \alpha_2 \cdots$ Thus

$$I = \int_{\mathcal{C}}F(z)\,e^{z(t-1/\sigma)} = 0. \quad \text{(F9)}$$

In what follows, the integral $\int_{C_i}F(z)e^{z(t-1/\sigma)}$ will be denoted by I_i. One can easily check that, by using Jordan's lemma:

$$\lim_{D\to\infty}I_2 = \lim_{D\to\infty}I_6 = \lim_{\epsilon\to 0}I_4 = 0. \quad \text{(F10)}$$

Therefore,

$$I_1 = -I_3 - I_5. \quad \text{(F11)}$$

Then we calculate the quantity $-I_3 - I_5$ by applying the residue theorem to the long rectangular contour delimited by $\mathcal{C}_3$ and $\mathcal{C}_5$ and covered in the opposite sense than in Fig. 12:

$$-I_3 - I_5 = 2i\pi\sum_{k=0}^{\infty}\text{Res}[F(z)e^{z(t-1/\sigma)},z_k]. \quad \text{(F12)}$$

In order to compute the residues, we apply the formula

$$\text{Res}[F(z)e^{z(t-1/\sigma)},z_k] = Az_k^{1-\nu}i^{-2\nu}\frac{J_\nu[iY(z_k)]}{J'_{-\nu}[iY(z_k)]}e^{z_k(t-1/\sigma)} \quad \text{(F13)}$$

(we need to verify *a posteriori* that all the poles are simple), and we use the relation

$$J'_\alpha(z) = \frac{\alpha}{z}J_\alpha(z) - J_{\alpha+1}(z). \quad \text{(F14)}$$

We eventually get

$$\chi^\sigma(t) = -\frac{1}{\overline{\langle\mathbf{T}\rangle}_T}\frac{d_fd_w}{\left(d_w^2-d_f^2\right)2^{2-2\nu}}\frac{\Gamma(\nu)}{\Gamma(2-\nu)}\sum_{k=0}^{\infty}\alpha_k^{3-2\nu}$$
$$\times\frac{J_\nu(\alpha_k)}{J_{-\nu+1}(\alpha_k)}\exp\left\{-\alpha_k^2\left[\frac{d_wd_f}{2\left(d_w^2-d_f^2\right)}\frac{t}{\overline{\mathbf{T}}_T}-\frac{1}{\sigma}\right]\right\}. \quad \text{(F15)}$$

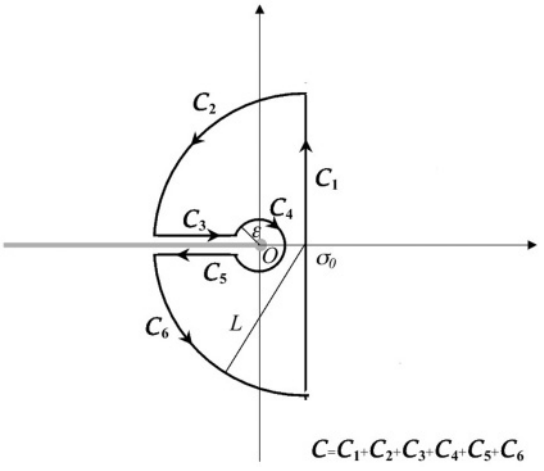

FIG. 12. Bromwich contour $\mathcal{C}$.

APPENDIX G: SOME USEFUL EXPRESSIONS

The FPT moments displayed in Sec. II B contain sums of the form

$$\mathcal{S}_{TT,n} = \sum_{k_1=1}^{N} \cdots \sum_{k_{n-1}=1}^{N} \sum_{k_n=1}^{N} H_{Tk_1} \ldots H_{k_{n-1}k_n} H_{k_nT} \quad \text{(G1)}$$

and of the form

$$\begin{aligned} \tilde{\mathcal{S}}_{TS,n} &= \sum_{k_1=1}^{N} \cdots \sum_{k_n=1}^{N} H_{Tk_1} \cdots H_{k_{n-1}k_n} \left(H_{k_nT} - H_{k_nS}\right) \\ &= \mathcal{S}_{TT,n} - \mathcal{S}_{TS,n}. \end{aligned} \quad \text{(G2)}$$

In this section we show that these sums can be rewritten in a simpler, more tractable form.

We present the detailed calculations for the particular sum

$$\mathcal{S}_{ji,1} = \sum_{k=1}^{N} H_{jk} H_{ki}. \quad \text{(G3)}$$

Let us replace the pseudo-Green function by its definition (6):

$$\mathcal{S}_{ji,1} = \sum_{n=0}^{\infty} \sum_{m=0}^{\infty} \sum_{k=1}^{N} \left[W_{jk}(n) - W_j^{\text{stat}}\right]\left[W_{kj}(m) - W_k^{\text{stat}}\right]. \quad \text{(G4)}$$

Since the random walk is Markovian, the propagator reads

$$\begin{aligned} \sum_{k=1}^{N} W_{jk}(n)\, W_{ki}(m) &= \sum_{k=1}^{N} W_{jk}(n+m|m)\, W_{ki}(m) \\ &= W_{ji}(n+m) \quad \forall\, i,j. \end{aligned} \quad \text{(G5)}$$

Using (G5), (A5), and (2), we have, for (G4),

$$\mathcal{S}_{ji,1} = \sum_{n=0}^{\infty} \sum_{m=0}^{\infty} \left[W_{ji}(n+m) - W_j^{\text{stat}}\right]. \quad \text{(G6)}$$

Introducing the variable $u = n + m$, we get

$$\mathcal{S}_{ji,1} = \sum_{u=0}^{\infty} \sum_{n=0}^{u} \left[W_{ji}(n) - W_j^{\text{stat}}\right], \quad \text{(G7)}$$

and finally

$$\mathcal{S}_{ji,1} = \sum_{u=0}^{\infty} u \left[W_{ji}(u) - W_j^{\text{stat}}\right]. \quad \text{(G8)}$$

In a similar way, it can be shown that

$$\mathcal{S}_{ji,k} = \sum_{u=0}^{\infty} u^k \left[W_{ji}(u) - W_j^{\text{stat}}\right]. \quad \text{(G9)}$$

This rewriting makes it clear that $S_{ji,k}$ can be computed as follows. Let us define the function F_{ji} by

$$F_{ji}(u) = W_{ji}(u) - W_j^{\text{stat}}. \quad \text{(G10)}$$

The sum $\mathcal{S}_{ji,n}$ is the nth moment of F_{ij}. It is then given by

$$\mathcal{S}_{ji,n} = (-1)^n\, n!\, \beta_{ji,n}, \quad \text{(G11)}$$

where the $\beta_{ji,n}$ are the coefficients of the power expansion of the discrete Laplace transform $\hat{F}_{ji}$ of F_{ji}, defined by

$$\hat{F}_{ji}(s) = \sum_{u=0}^{\infty} F_{ji}(u) e^{-s\,u}, \quad \text{(G12)}$$

as s tends toward zero:

$$\hat{F}_{ji}(s) = \sum_{n=0}^{\infty} \beta_{ji,n} s^n. \quad \text{(G13)}$$

[1] S. Rice, *Diffusion-Limited Reactions* (Elsevier, Amsterdam, 1985).
[2] R. Kopelman, Science **241**, 1620 (1988).
[3] M. F. Shlesinger, G. M. Zaslavsky, and J. Klafter, Nature (London) **363**, 31 (1993).
[4] Z. Schuss, A. Singer, and D. Holcman, Proc. Natl. Acad. Sci. USA **104**, 16098 (2007).
[5] L. Mirny, Nature Phys. **4**, 93 (2008).
[6] O. Benichou, C. Loverdo, M. Moreau, and R. Voituriez, Phys Chem Chem Phys **10**, 7059 (2008).
[7] O. G. Berg, R. B. Winter, and P. H. von Hippel, Biochemistry **20**, 6929 (1981).
[8] M. Slutsky and L. A. Mirny, Biophys. J. **87**, 4021 (2004).
[9] M. Coppey, O. Benichou, R. Voituriez, and M. Moreau, Biophys. J. **87**, 1640 (2004).
[10] M. A. Lomholt, T. Ambjornsson, and R. Metzler, Phys. Rev. Lett. **95**, 260603 (2005).
[11] I. Eliazar, T. Koren, and J. Klafter, J. Phys. Condens. Matter **19**, 065140 (2007).
[12] T. Hu, A. Y. Grosberg, and B. I. Shklovskii, Biophys. J. **90**, 2731 (2006).
[13] M. Sheinman and Y. Kafri, Phys. Biol. **6**, 016003 (2009).
[14] O. Benichou, Y. Kafri, M. Sheinman, and R. Voituriez, Phys. Rev. Lett. **103**, 138102 (2009).
[15] C. Loverdo, O. Benichou, R. Voituriez, A. Biebricher, I. Bonnet, and P. Desbiolles, Phys. Rev. Lett. **102**, 188101 (2009).
[16] S. Condamin, O. Benichou, and M. Moreau, Phys. Rev. Lett. **95**, 260601 (2005).
[17] S. Condamin *et al.*, Nature (London) **450**, 77 (2007); O. Benichou, B. Meyer, V. Tejedor, and R. Voituriez, Phys. Rev. Lett. **101**, 130601 (2008); O. Benichou and R. Voituriez, Nature (London) **100**, 168105 (2008).
[18] O. Bénichou, C. Chevalier, J. Klafter, B. Meyer, and R. Voituriez, Nat. Chem. **2**, 472 (2010).
[19] D. Ben-Avraham and S. Havlin, *Diffusion and Reactions in Fractals and Disordered Systems* (Cambridge University Press, Cambridge, UK, 2000).
[20] J.-P. Bouchaud and A. Georges, Phys. Rep. **195**, 127 (1990).

[21] R. P. Parson and R. Kopelman, Chem. Phys. Lett. **87**, 528 (1982).
[22] R. Metzler and J. Klafter, J. Phys. A **37** (2004).
[23] S. B. Zimmerman and A. P. Minton, Annu. Rev. Biophys. Biomol. Struct. **22**, 27 (1993).
[24] H.-X. Zhou, G. Rivas, and A. P. Minton, Annu. Rev. Biophys. **37**, 375 (2008).
[25] M. J. Saxton, Biophys. J. **92**, 1178 (2007).
[26] M. J. Saxton, Biophys. J. **94**, 760 (2008).
[27] S. Condamin, V. Tejedor, R. Voituriez, O. Benichou, and J. Klafter, Proc. Natl. Acad. Sci. USA **105**, 5675 (2008).
[28] N. Malchus and M. Weiss, J. Fluoresc. **20**, 19 (2010).
[29] J. Szymanski and M. Weiss, Phys. Rev. Lett. **103**, 038102 (2009).
[30] O. Benichou, C. Chevalier, B. Meyer, and R. Voituriez, Phys. Rev. Lett. **106**, 038102 (2011).
[31] D. Lebedev, M. Filatov, A. Kuklin, A. Islamov, J. Stellbrink, R. Pantina, Y. Denisov, B. Toperverg, and V. Isaev-Ivanov, Crystallogr. Rep. **53**, 110 (2008).
[32] A. Bancaud, S. Huet, N. Daigle, J. Mozziconacci, J. Beaudouin, and J. Ellenberg, EMBO J. **28**, 3785 (2009).
[33] E. Lieberman-Aiden *et al*., Science **326**, 289 (2009).
[34] G. Barton, *Elements of Green's Functions and Propagation* (Oxford Science Publications, Oxford, 1989).
[35] V. Tejedor, O. Bénichou, and R. Voituriez, Phys. Rev. E **80**, 065104 (2009).
[36] P. G. de Gennes, J. Chem. Phys. **76**, 3316 (1982).
[37] B. D. Hughes, *Random Walks and Random Environments* (Oxford Science Publication, Oxford, 1995).
[38] B. O'Shaughnessy and I. Procaccia, Phys. Rev. Lett. **54**, 455 (1985).
[39] B. O'Shaughnessy and I. Procaccia, Phys. Rev. A **32**, 3073 (1985).
[40] E. Barkai, Phys. Rev. E **63**, 046118 (2001).
[41] S. Condamin, O. Benichou, and J. Klafter, Phys. Rev. Lett. **98**, 250602 (2007).
[42] S. Condamin, O. Benichou, and M. Moreau, Phys. Rev. E. Stat. Nonlin. Soft Matter. Phys. **75**, 021111 (2007).
[43] S. Condamin and O. Benichou, J. Chem. Phys. **124**, 206103 (2006).
[44] P. Argyrakis, A. Milchev, V. Pereyra, and K. Kehr, Phys. Rev. E **52**, 3623 (1995).
[45] C. P. Haynes and A. P. Roberts, Phys. Rev. E **78**, 041111 (2008).
[46] E. Agliari, Phys. Rev. E **77**, 011128 (2008).
[47] E. W. Montroll, J. Math. Phys. **10**, 753 (1969).
[48] J. J. Kozak and V. Balakrishnan, Phys. Rev. E **65**, 021105 (2002).
[49] S. Redner, *A Guide to First-Passage Processes* (Cambridge University Press, New York, 2001).